THE ASTROPHYSICAL JOURNAL, 300:522–539, 1986 January 15

ENERGETIC RADIATION FROM RAPIDLY SPINNING PULSARS. II. VELA AND CRAB

K. S. CHENG,[1] C. HO,[2] AND M. RUDERMAN[3]
Department of Physics, Columbia University
Received 1985 May 17; accepted 1985 July 16

ABSTRACT

The growth of charge-depleted regions (gaps) in the outer magnetosphere of rapidly spinning magnetized neutron stars is limited by $e^{\pm}$ production. In the Vela pulsar a pair of e^+ and e^- created within the gap (primaries) are accelerated in opposite directions to extreme relativistic energies. The primary e^-/e^+ produce primary γ-rays through inverse Compton scattering on IR photons. Primary γ-rays are sufficiently energetic to produce (secondary) $e^{\pm}$ pairs in collisions with this same IR photon flux. Secondary synchrotron radiation by these pairs gives crossed fan beams of γ-rays and weaker ones of X-rays. Collisions of the hard secondary γ-rays with the secondary crossed beam soft X-rays give a large flux of lower energy $e^{\pm}$ (tertiary) pairs which fill much of the outer magnetosphere. It is the (tertiary) IR synchrotron radiation from tertiary pairs through the outer gap which initiates the entire series of pair production processes. For Vela, the calculated observable consequences include (*a*) twin cusped γ-ray pulses with photon spectrum $F(\omega) \approx \omega^{-3/2} \ln (3\ \mathrm{GeV}/\hbar\omega)$ from 3 GeV to about 10^2 KeV; (*b*) total fan beam radiated power 10^{-2} the pulsar spin-down energy loss rate; (*c*) an X-ray spectrum $F(\omega) \approx \omega^{-2/3}$ below 10^2 KeV; (*d*) weak, more closely spaced twin optical pulses from the tertiary radiation with power 10^{-5} that of the secondary γ-rays; (*e*) and $e^{\pm}$ outflow of 10^{36} s^{-1}; (*f*) a double pulse of 10^{12}–10^{13} eV γ-rays with about 10^{-2} the γ-ray power. Model Crab pulsar emissions are considered with emphasis on differences from those of Vela. Crab primary outer gap e^+/e^- lose most of their energy to curvature γ-rays, which convert to $e^{\pm}$ pairs in collisions with X-rays. These X-rays come from the synchrotron (secondary) emission from such (secondary) pairs created beyond the gap boundary. Inverse Compton scattering of secondary $e^{\pm}$ on the secondary X-rays boosts a fraction to γ-rays. The combination of secondary synchrotron and inverse Compton emission into twin fan beams gives the Crab pulsar spectrum from optical to GeV energies. Other mechanisms give the Crab's double pulsed radio and 10^{12}–10^{13} eV emission and the possibility of 10^{15} eV nucleon beams.

Subject headings: hydromagnetics — pulsars — radiation mechanisms — stars: neutron

I. INTRODUCTION

In Cheng, Ho, and Ruderman (1985, hereafter CHR I), it was shown how assumed global current flow in the outer magnetosphere of a spinning magnetized neutron star can result in a specially located outer magnetosphere gap with large charge depletion. Within this gap there is a strong electric field along $\boldsymbol{B}(\boldsymbol{E}\cdot\hat{\boldsymbol{B}})$ which extends with nearly constant strength from the beginning of the gap (near the "null surface" where $\boldsymbol{\Omega}\cdot\boldsymbol{B}\equiv 0$) out through the light cylinder. For the Crab and Vela pulsars the potential drop along $\boldsymbol{B}$ in the outer gap is of order 10^{15} V. The gap grows until the $e^{\pm}$ production which it generates is sufficient to limit its own size and to supply enough charge to keep $\boldsymbol{E}\cdot\hat{\boldsymbol{B}}\approx 0$ in the rest of the outer magnetosphere without quenching it within its own. This steady charge replenishment includes the continual creation of the charged layer which forms the flowing upper boundary of the gap itself. That boundary region, no longer the infinitesimally thin outer boundary of the static model, screens the gap charge deficits electric field so that $\boldsymbol{E}\cdot\hat{\boldsymbol{B}}\approx 0$ outside the gap. The steady state outer magnetosphere consists of the three regions (Fig. 1):

I. the gap itself with the large $\boldsymbol{E}\cdot\hat{\boldsymbol{B}}$ of equation (3.10) and (3.11) of CHR I. In it e^+ and e^- will be oppositely accelerated to ultrarelativistic energies until limited by loss to γ-ray emission. These γ-rays, whose source can in principle be the electron's centripetal acceleration from the $\boldsymbol{B}$ field curvature (in the case of the Crab) or inverse Compton scattering (in the case of Vela), will partly convert within the gap; they will make more pairs which will separate and produce a net charge in the gap and repeat the process until enough net charge is created to terminate the gap. Near and just beyond this region we continue to have pair creation from these extremely energetic γ-rays created in the gap (primary γ-rays) which originated from gap-accelerated $e^{\pm}$ (primary $e^{\pm}$). These create

II. a boundary layer region in which the primary γ-rays create secondary $e^{\pm}$ pairs which no longer move in the large $\boldsymbol{E}\cdot\hat{\boldsymbol{B}}$ of the gap. The small remnant $\boldsymbol{E}\cdot\hat{\boldsymbol{B}}$ in (II) will separate only the fraction of the secondary pairs (by reversing the velocity of some e^- or e^+) needed to establish the gap's "upper" charged boundary. The secondary pairs are created with very high energy, so that they also radiate energetic γ-rays and X-rays (secondary photons). A small fraction of these X-rays may (with great uncertainty) illuminate the gap and sustain the gap in the case of the Crab. In addition, because primary e^- and e^+ move in opposite directions, so do the primary γ-rays, the secondary pairs they create and, thus, the secondary γ-rays: the crossed beams of secondary γ-rays (and X-rays) will create yet another generation of $e^{\pm}$ pairs (tertiary $e^{\pm}$) beyond the boundary layer region in

III. the tertiary pair–filled outer magnetosphere well beyond the gap. Here most pairs are not created with nearly enough energy to produce γ-rays or even X-rays. The tertiary

[1] Present address: Department of Physics, University of Illinois, Urbana.
[2] Also Astronomy Department, University of California, Berkeley.
[3] Also Theoretical Group, Stanford Linear Accelerator Center, Stanford, California.

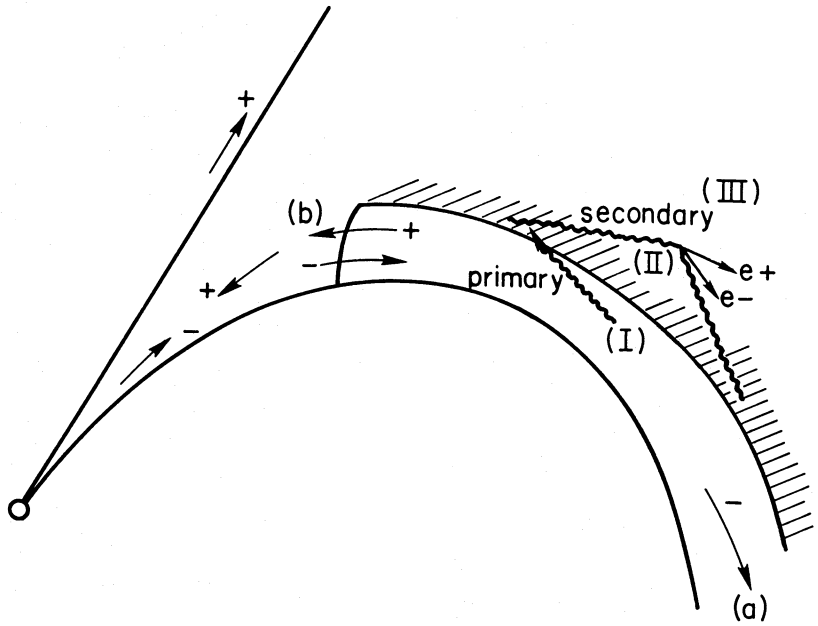

FIG. 1.—Schematic representation for positions of primary (I), secondary (II), and tertiary (III) regions associated with an outer gap. The current flow on $\boldsymbol{B}$ field lines through an outer gap begins at (b) and extends through (a) for $\rho_0 > 0$ above the polar cap. For an oppositely spinning pulsar with the same $\boldsymbol{B}$, $\rho_0 < 0$ and all signs of charges would be reversed.

electromagnetic radiation from this region is mainly soft synchrotron radiation (IR for Vela parameters) which floods the entire outer magnetosphere including the gap itself. (The more energetic, less abundant, flux of secondary photons from the boundary layer region (region [II]) are less likely to pass through the gap.) Our model for young pulsars like Vela will have a high enough density of tertiary IR (10^{-1} to 1 eV) photons within their outer magnetosphere gaps to sustain sufficient inverse Compton collisions of primary $e^{\pm}$ in the gap to give the needed primary γ-ray (10^{12}–10^{13} eV) production. The necessary conversion of those primary γ-rays into $e^{\pm}$ pairs in both (I) and (II) comes mainly from collisions with these same tertiary IR photons. But for the Crab, a small fraction of leakage of the secondary X-rays into the gap may be able to sustain the gap closures by supporting $e^{\pm}$ creation of primary curvature γ-rays.

The processes in regions (I) and (II) (and [III]) are mutually dependent. Power is taken from (I) by primary γ-rays and transferred to (II), where it appears in superenergetic $e^{\pm}$ secondary pairs. The secondary radiation from these forms most of the observable fan beams discussed in CHR I, § IV. Most of it escapes the magnetosphere. In Vela only a very small fraction is absorbed in creating the tertiary pairs which radiate low power but an abundant uncollimated flux of IR photons which plays a crucial role (at least in Vela) in transferring power out of the gap and in continually maintaining its charged screening boundary layer. The above bootstrap magnetosphere model, in which (I) controls (II) which controls (III) which controls (I), does not suggest a unique starting place for a detailed semi-quantitative study. We shall look first at some of the relevant processes in (III) (which depend on the spectrum and intensity of the crossed γ-ray and X-ray beams from [II] which create the $e^{\pm}$ pairs in [III]). For the Crab, there is less certainty regarding their exact interdependence because of the great uncertainty in geometry which determines the availability of those secondary X-rays (from [II]) in the (I) which convert the primary curvature photon and initiate the whole charge production processes.

The mechanisms for the production of these secondary γ-rays can differ in important details between Vela and the more rapidly spinning Crab pulsar. For Vela some observable γ-radiation above 10^{12} eV is expected to originate from inverse Compton scattering, but all other electromagnetic radiation—from several GeV to optical frequencies—is synchrotron emission. In Vela, but not in the Crab, the optical synchrotron radiation comes from a region closer to the star than does the higher energy radiation. This causes it to be much fainter than the former and to have a smaller pulse separation. The calculation of the predicted Vela spectrum is relatively uncomplicated and agrees with present observations. For the Crab, however, observed γ-radiation comes from inverse Compton scattering, while synchrotron radiation by these same scattering electrons gives the spectrum from hard X-ray through optical and IR. The model-based emission spectrum agrees well with that observed for the Crab over this entire range.

Section II discusses how the flow of e^+ and e^- through the gap sustains large pair production there through a mechanism which, for Vela, begins with the inverse Compton scattering of gap-accelerated $e^-(e^+)$ on the soft IR flux which passes through the gap. This large pair production limits the gap's width and potential drop and also initiates processes which create $e^{\pm}$ plasma elsewhere. The latter prevents charge depletion along field lines on which it is created and allows the return current to the star to be maintained even if no charge enters the magnetosphere through the light cylinder. Section III considers consequences of pair production well beyond the gap created by these "secondary" γ-rays. It is shown in § III how pairs move in the outer magnetosphere and produce a copious flux of soft (IR) photons which pass back through the gap. Section IV estimates the necessary gap power, soft photon flux, and other gap parameters which follow from self-consistency for Vela. The scaling of these quantities with pulsar

spin rate and magnetic field is discussed. Section V contains a calculation of the spectrum of the emitted radiation beams from the Vela pulsar in the γ-ray, X-ray, and optical regimes, and the spectrum is compared to observations. Section VI considers the self-consistent "dynamic" gap of the Crab pulsar. Section VII gives the double-pulsed emission spectrum which results from it. Section VIII contains (*a*) a calculation of the expected power in Vela's double pulses of 10^{12}–10^{13} eV γ-rays (and in the Crab, where one of the pulses can be strongly absorbed in passing back through the magnetosphere), (*b*) remarks on the relevance of the model for radio emission from Vela and the Crab, (*c*) the total flux of $e^{\pm}$ pairs created by outer gap–initiated processes in the outer magnetosphere which ultimately flow out through the light cylinder, (*d*) the origin and power of high-power 10^{15} eV nucleon beams from rapidly spinning pulsars and possible consequences for superenergetic ($\sim 10^{15}$ eV γ-ray [or neutrino] detection), (*e*) the expected polar cap heating in Vela from its outer gaps and other processes and the implications of constraints from observed upper bounds to such heating, and (*f*) some remarks about other pulsars or white dwarfs whose product of (spin-rate)^2(magnetic dipole moment) is comparable to that of the Crab or Vela pulsars.

We shall use the notation of CHR I, § V in which the time scale τ for synchrotron radiation of a relativistically spiraling $e^+(e^-)$ is

$$\frac{1}{\tau} \approx \left(\frac{\gamma_\perp}{\gamma_\parallel}\right)\left(\frac{e^2}{mc^3}\right)\omega_B^2 \approx 30\left(\frac{\gamma_\perp}{\gamma_\parallel}\right)B_5^2 \text{ sec}^{-1}, \tag{1.1}$$

with

$$\omega_B \equiv eB/mc, \tag{1.2}$$

$$\gamma \equiv E/mc^2, \tag{1.3}$$

$$\gamma_\perp \equiv \sqrt{(p_\perp/mc)^2 + 1} \approx \gamma \sin\theta, \tag{1.4}$$

$$\gamma_\parallel = \frac{\gamma}{\gamma_\perp} \approx \frac{1}{\sin\theta}. \tag{1.5}$$

II. OUTER GAP CONTROL MECHANISMS

In the transition from a static to a steady state outer magnetosphere with the current distribution of Figure 1 of CHR I, the outer gap of Figures 2 and 3 of CHR I will expand (or contract) in width until $e^{\pm}$ pair production by it and subsequent charge separation produce the outer (open field line) boundary layer charge needed to terminate the gap. The resulting stabilized "dynamic" gap and charged outer boundary layer have a structure which is different from that of a "static" one. Most significantly, while the static solution permits a gap of arbitrary width (and thus of $\boldsymbol{E}\cdot\hat{\boldsymbol{B}}$), the dynamic gap is stabilized only at those values of a which sustain just the needed $e^{\pm}$ pair production within it and in its open field line boundary region. The required outer gap pair production could, in principle, be sustained in at least four ways depending on pulsar parameters.

A. Pair production by primary-curvature γ-rays from gap-accelerated e^-/e^+ along $\boldsymbol{B}$. Radiation reaction limits the primary $e^-(e^+)$ energy to E_p to

$$\gamma_1 \equiv \frac{E_p}{mc^2} \le \left(\frac{\boldsymbol{E}\cdot\hat{\boldsymbol{B}}}{e}s^2\right)^{1/4}, \tag{2.1}$$

with s the magnetic field radius of curvature. The maximum curvature γ-ray energy from such e^-/e^+, $\hbar\omega_m$, is then given by

$$\frac{\hbar\omega_m}{mc^2} \equiv \gamma_m = \left(\frac{\boldsymbol{E}\cdot\hat{\boldsymbol{B}}}{e}\right)^{3/4}\frac{\hbar\sqrt{s}}{mc}, \tag{2.2}$$

with $\boldsymbol{E}\cdot\hat{\boldsymbol{B}}$ from equation (3.11) of CHR I, $\gamma_m \le 10^4 f^{3/2}$ for Vela and $\gamma_m < 10^5 f^{3/2}$ for the Crab pulsar, with f the ratio of gap half-width $a/2$ to s. To materialize into Sturrock pairs (Sturrock 1971) in the gap $\boldsymbol{B}$, γ_m must be such that

$$\gamma_m B_{12}\phi \ge 1, \tag{2.3}$$

with ϕ the angle between the materializing γ-ray and $\boldsymbol{B}$. The pair production probability decreases very sharply ($\sim\exp[-4m^2c^3/3\gamma\hbar eB]$) below the B of equation (2.3). For many generations of $e^{\pm}$ pairs ($\gamma\to e^{\pm}\to\gamma\to e^{\pm}\ldots$) within the gap or around its outer boundary, the conversion mean free path is much less than s and thus $\phi \ll 1$. Thus $B_{12} \gg \gamma_m^{-1}$ must be satisfied for Sturrock pair creation to be important in outer gap electrodynamics. For Vela outer gap parameters near its light cylinder (§ IV) $B_{12} \approx 10^{-8}$ and $\gamma_m < 10^4$, so that the inequality is not satisfied. For the Crab pulsar it probably still fails by at least an order of magnitude. (Sturrock pairs in an outer gap may be relevant for pulsars spinning much more rapidly than the Crab, so that the outer magnetosphere magnetic field [$\propto\Omega^3$] is very much larger. We shall not consider it further here.)

B. Pair production by primary curvature γ-rays in the gap incident on thermal X-rays from the neutron star. For Vela the upper bound to any steady surface thermal emission $\lesssim 10^{33}$ ergs s^{-1} at X-ray energies of order 1 KeV. At a distance $\sim 5\times 10^8$ cm, (the maximum number density of such photons) $\times$ ($s \approx 5\times 10^8$ cm) $\times$ ($\sigma_{\gamma+x\to e^++e^-} \approx 10^{-25}$ cm^2) gives an optical depth $\sim 3\times 10^{-2}$. If thermal X-ray emission from the strongly magnetized rotating neutron star surface is, as expected, strongly modulated, observation gives a stronger upper bound to surface thermal X-ray emission and an optical depth for pair production by curvature γ-rays through the gap of less than 10^{-3}. Therefore this process is certainly ineffective for a Vela pulsar outer gap. For the younger Crab this is less certain, because observations alone do not distinguish between a possibly strongly modulated thermal X-ray emission and a strong nonthermal one from the outer magnetosphere. However, similarities in the observed high-energy power and spectra of the Crab and Vela pulsars suggest that similar emission mechanisms are involved. We shall therefore presume that also in the Crab pair production, the thermal X-ray flux in the outer gap is unimportant.

C. Pair production by primary-curvature γ-rays incident on secondary X-rays which penetrate into the gap. We will see in § III that geometrical constraints are expected to make it difficult for secondary X-rays to pass through the gap (but not the very much softer and much more abundant " tertiary " flux). For the Vela pulsar there is the additional observational constraint, mentioned above, on the weak intensity of any beamed nonthermal X-ray flux around 1 KeV. However, even a very small maximum "optical" depth for $e^{\pm}$ conversion of curvature γ-rays in the gap ($\sim 10^{-3}$) could, in principle, sustain the pair production needed to terminate an outer gap and sustain the current flow of Figure 1. In a passage along the entire length of the gap, each e^-/e^+ would radiated $N_\gamma = e^2\gamma_2/\hbar c$ curvature γ-rays with the γ_1 of equation (2.1). N_γ is typically $\sim 10^5$, so that up to 10^2 γ-rays could then convert in a thick gap and $10^2(a/s)^{1/2}$ in a thin one ($a \ll s$). For the Vela pulsar,

this gap $e^{\pm}$ pair production process (C) will be presumed to be unimportant for two reasons: (1) in Vela, process (D) below takes much more power from the gap than could process (C) even if a large fraction of Vela's secondary X-rays could flow through the gap; (2) because of the small gap "optical" depth, the observed beamed spectrum would be curvature radiation directly from the gap emitted by e^{+}/e^{-} moving with the constant γ_1 of equation (2.1). This is inconsistent with observations of Vela's γ-rays emission spectrum. The observed Vela pulsar high-energy photon spectrum between $\hbar\omega_2 \approx$ several GeV and $\hbar\omega_1 \approx$ several MeV is approximately

$$I(\omega) \approx 10^{35}\omega_2^{\nu-1}\omega^{-\nu} \text{ ergs s}^{-1} . \tag{2.4}$$

Very roughly, $\nu \approx \frac{2}{3}$. The energy spectrum of the primary e^{+}/e^{-} particle current through the gap whose curvature emission is that of equation (2.4) is

$$f(\gamma_1) \approx \frac{10^{35} \text{ ergs s}^{-1}}{(e^2/s)(\omega_2 s/c)^{1/3}\gamma_1^{3\nu+2}} , \tag{2.5}$$

for $(\omega_2 s/c)^{1/3} \geq \gamma_1 > (\omega_1 s/c)^{1/3}$. Then F_1, the total primary e^{+}/e^{-} flow through the gap, would have to satisfy (for $\nu \approx \frac{2}{3}$) the inequality

$$F_1 \geq \frac{10^{35} \text{ ergs s}^{-1}}{(e_2/s)(\omega_1 s/c)(\omega_2 s/c)^{1/3}} \approx 10^{35} \text{ s}^{-1} . \tag{2.6}$$

However, the charge-separated flow through the outer gap must not exceed the total flow through the Vela neutron star, approximately 10^{33} s^{-1}. Therefore the maximum particle flow through the Vela outer gap is at least two orders of magnitude too small to supply the lower end of the Vela pulsar's γ-ray spectrum if the source of those γ-rays is curvature radiation from the gap. For both of the above reasons, we shall not consider this mechanism further as a candidate for sustaining and limiting the Vela pulsar's outer magnetosphere gap. For the Crab pulsar, however, the situation is more complicated, and both the above counterarguments to mechanism (C) fail. The observed Crab pulsar X-ray emission can be optically thick for $e^{\pm}$ production by gap curvature γ-rays with $\hbar\omega \gtrsim 1$ GeV. Such secondary $e^{\pm}$ pairs can then be a powerful source of much lower energy photons. Therefore the observed γ-ray spectrum of the Crab pulsar could be quite different from one emitted from the gap as curvature radiation. In addition, the Crab pulsar's magnetic field in its outer magnetosphere is about 30 times greater than that of Vela, and thus tertiary synchrotron radiation from regions (II) and (III) is emitted 10^3 times faster. Therefore, magnetic mirror reflection of inward-flowing synchrotron-radiating tertiary pairs is marginal for the Crab pulsar, and the strong IR flux deep in Vela's outer gap may not be present in that of the Crab's. The Crab outer gap will be considered in § VI and its radiation spectrum in § VII.

D. Pair production by primary γ-rays produced from the inverse Compton scattering of primary e^{+}/e^{-} on the abundant soft secondary (tertiary) photons which flow through the gap. The primary γ-rays can make $e^{\pm}$ pairs by collisions with this same tertiary photon flux. This is the only remaining candidate for controlling Vela's outer gap and, depending on the detailed geometry, perhaps that of the Crab. We shall consider the tertiary photon distribution for Vela in § III and its relatively uncomplicated consequences in more detail in §§ IV and V. The application to the Crab pulsar will also be discussed there and in §§ VI and VII.

III. THE TERTIARY PHOTON SPECTRUM AND GEOMETRICAL CONSIDERATIONS

The total spectrum and flux of tertiary soft photons produced in (III) of Figure 1 depends on the energy distribution of the pairs created there from $\gamma + \gamma \rightarrow e^{+} + e^{-}$ by the flux of secondary γ-rays and X-rays in each of the crossed beams from (II). The γ-γ cross section (Heitler 1960) has a threshold center of mass energy $E_{\text{CM}} = 2mc^2$, peaks at $\sim 3mc^2$ with a fairly flat plateau, and falls off as $E_{\text{CM}}^{-2} \ln E_{\text{CM}}$ at much higher energies. Most of the pairs are created with $E_{\text{CM}} \approx (3 \pm 1)mc^2$. As discussed in § V, the intensity of the secondary radiation has a power law spectrum $I(\omega) \approx \omega^{-1/2}$ for the energies $E = \hbar\omega$ which gives most of the $e^{\pm}$ pair production in (III), and this gives a simple energy spectrum for the tertiary $e^{\pm}$ pairs they produce. The energy of the tertiary $e^{\pm}$ pair in (III) is essentially that of the most energetic photon of the secondary photon pair which produced it. The mean free path for $e^{\pm}$ conversion of the secondary photons in (III) is much greater than the extent of the pulsar magnetosphere ($\sim c/\Omega$) for almost all the secondary photons (for all secondary γ-rays in Vela, and for those of energy below 1 GeV in the Crab). Therefore the energy spectrum of the $e^{\pm}$ produced in (III), $F_3(E)$, is proportional to the product of $I_2(\omega)/\hbar\omega$ (the photon number flux of very energetic secondaries in one beam) and the number flux of secondary photons in the crossing beam whose energies (E') are such that $mc^2 \lesssim (EE')^{1/2} \lesssim$ several mc^2. Then the E dependence of the tertiary $e^{\pm}$ flux in (III) is given by

$$F_3(E) \propto \left[\frac{I_2(E/\hbar)}{E}\right]\left[\frac{I_2(m^2c^4/\hbar E)}{mc^2/E}\right]\left(\frac{mc^2}{E}\right) \tag{3.1}$$

(except when $E \approx E' \approx mc^2$. But from equation [5.1] of CHR I, such low-energy pairs with $\gamma_{\perp} \approx 1$ will not have time to radiate enough to dominate the synchrotron radiation in the outer magnetosphere of Vela [$B_5 < 1$] and similar pulsars. In addition, their very soft synchrotron radiation with $\omega \approx \omega_B$ will be strongly depressed by self-absorption.) Because $I_2(E)$ from the secondaries is proportional to the time-integrated synchrotron intensity from a single electron

$$I(\omega) \propto \frac{mc^2\gamma_{\parallel}^{1/2}}{(\omega_B\omega)^{1/2}} , \tag{3.2}$$

equation (3.1) gives

$$F_3(E) \propto 1/E , \tag{3.3}$$

for $e^{\pm}$ energies E up to an E_{max} of order several GeV or greater.

Most of the soft tertiary photons whose spectrum is described by equations (3.1) and (3.3) (especially that from outward flowing pairs) cannot penetrate deeply into the gap ([I]) because of geometrical constraints. An energetic γ-ray with $\hbar\omega \gg mc^2$ which makes an $e^{\pm}$ pair by colliding with a much lower energy ($\sim m^2c^4/\hbar\omega \ll mc^2$) photon will make a pair with e^{+} and e^{-} initial momenta almost parallel to its own. If that photon has an angle of incidence θ with respect to the local magnetic field $\boldsymbol{B}$, then, as long as $\gamma_{\perp} > 1$, so will the thin cone of synchrotron radiation from the $e^{\pm}$ pair which it makes. In this way there is some "memory" in each generation of photons of the location within the gap of the emission field line of the original γ-ray (Fig. 2). Because that initial γ-ray is emitted essentially parallel to its local $\boldsymbol{B}$ direction, the tertiary e^{+}/e^{-} created far above the gap in (II) will generally have a $\gamma_{\parallel}$ which does not permit their synchrotron radiation to flow

through most of the gap below. This severely constrains the number density of available low-energy photons inside the gap which is essential for the gap charge reproduction.

Because of the divergence of $\boldsymbol{B}$ field lines with distance from the neutron star, outwardly directed secondary γ-rays make tertiary pairs whose synchrotron radiation does not enter into the gap, but (secondary) tertiary pairs moving inward could in principle illuminate the gap at its inner end even more deeply then the position of the $\boldsymbol{B}$-field line on which their ancestral primary γ-ray was emitted (see Fig. 2). Nevertheless, the intensity of tertiary radiation in the gap from those pairs will be much less than it is at the upper boundary of the gap and beyond in region (II). However, much of the tertiary synchrotron radiation does flow through the entire gap because of the magnetic mirroring from converging $\boldsymbol{B}$-field lines, which ultimately reverses the direction of the inward-flowing tertiary $e^{\pm}$ pairs. The prompt initial burst of synchrotron radiation from newly created inwardly flowing tertiary pairs diminishes their $\gamma_{\perp}$ but does not affect their $\gamma_{\parallel}$. However, the convergence of the outer magnetosphere guiding $\boldsymbol{B}$-field for the flowing pairs acts to decrease $\gamma_{\parallel}$ and increase $\gamma_{\perp}$ while keeping $\gamma_{\perp}\gamma_{\parallel}$ constant. The adiabatic invariant (for $\gamma_{\perp} \gg 1$) is $B\gamma_{\perp}^{-2} \propto B\gamma_{\parallel}^{2} \approx$ constant. The initial $\gamma_{\parallel}$ of tertiary pairs in (III) is typically more than one but less than several. Since $\boldsymbol{B}$ along the length of the gap is expected to vary by more than an order of magnitude, the $\gamma_{\parallel}$ of the inwardly flowing pairs will drop to unity, and the $e^{\pm}$ inwardly flowing velocity $v_{\parallel} = c(1 - \gamma_{\parallel}^{-2})^{1/2}$ will fall to zero and reverse: the inward flowing pairs will be reflected outward and leave the magnetosphere. During this reversal, since $v_{\parallel}$ passes through zero, the tertiary synchrotron photons will be radiated through directions around and including that normal to the local $\boldsymbol{B}$. About half of that radiation will, therefore, pass through the gap below. This is the main source of tertiary photons deep in the gap. These photons will not include large contributions from those whose frequency ω greatly exceeds the characteristic synchrotron frequency for $\gamma_{\perp} = \hat{\gamma}_{\perp}$ of equation (5.6) of CHR I:

$$\omega_c = \gamma_{\perp}^2 \gamma_{\parallel} \omega_B \approx \left(\frac{\gamma_{\parallel}^3}{\tau^2 \omega_B^3}\right)\left(\frac{mc^3}{e^2}\right)^2 , \tag{3.4}$$

with residence time τ a significant fraction of $c\Omega^{-1}v_{\parallel}^{-1}$ (so that $\tau \approx \Omega^{-1}$). The synchrotron radiation with $\omega > \omega_c$, which is radiated by the more energetic tertiary $e^{\pm}$ pairs just after they are created and before they can move inward to reach the region in which they will be reflected, will be ignored in our estimates of the flux and spectrum of tertiary photons which penetrate deeply into the gap. (We note further from equation (3.4) that for the reflected $e^{\pm}$ the maximum photon flux emission occurs at the turnaround, where $\gamma_{\parallel} = 1$ is a minimum and ω_B is a maximum.) Then from equation (3.2) the energy distribution of those tertiary pairs which radiate into the gap while their $\gamma_{\parallel} \rightarrow 1$ and $v_{\parallel}$ reverses is

$$F_3(E) = A/E , \tag{3.5}$$

for $E < E_c$ defined by

$$\omega_{\rm IR} = \omega_c = \left(\frac{E_c}{mc^2}\right)^2 \gamma_{\parallel}\, \omega_B \tag{3.6}$$

and an additional

$$F_3(E) = A \ln\left[\frac{E_{\rm max}(3)}{E_c}\right] \delta(E - E_c) , \tag{3.7}$$

from tertiary pairs whose initial energies $\hat{E}$ were in the range $E_c < \hat{E} < E_{\rm max}$, the maximum tertiary $e^{\pm}$ energy. An $e^{-}(e^{+})$ radiates with an approximately power spectrum

$$\hat{I}(\omega) \approx \frac{e^2}{c}\left(\frac{\omega\omega_B^2}{\gamma_{\parallel}^4 \gamma_{\perp}^2}\right)^{1/3} \text{ for } \omega < \omega_{\rm IR} \tag{3.8}$$

and

$$\hat{I}(\omega) \approx 0 \text{ for } \omega > \omega_{\rm IR} . \tag{3.9}$$

Then from equations (3.5), (3.6), (3.8), and (3.9) the tertiary soft photon spectrum in the gap has an ω dependence

$$I_3(\omega) \approx \begin{cases} 1 - \left(\dfrac{\omega}{\omega_{\rm IR}}\right)^{1/3} + \dfrac{1}{3}\left(\dfrac{\omega}{\omega_B}\right)^{1/3} \ln\left(\dfrac{\omega_{\rm max}(3)}{\omega_{\rm IR}}\right), & \omega < \omega_{\rm IR} , \\ 0 , & \omega > \omega_{\rm IR} , \end{cases} \tag{3.10}$$

with $\omega_{\rm max}(3)$ the maximum energy of tertiary synchrotron photons. Equation (3.10) gives a rather flat spectrum below the $\omega_{\rm IR}$ cutoff. This spectrum supports the assumption made in equation (6.2) of CHR I for the model gap electrodynamic solution. Both self-absorption by the radiating tertiary pairs and the failure of the continuum approximation at $\omega \approx \omega_B$ will introduce a low-frequency cutoff at some $\omega = \omega_0 \ll \omega_{\rm IR}$ for Vela. For the Crab, where $\omega_{\rm IR}$ of equation (3.4) is less than ω_B, the soft spectrum in the gap is closer to monoenergetic than it is for Vela.

As we will see in § IV, there is a sufficient density of soft tertiary photons in the gap that the mean free path for inverse Compton scattering of gap-accelerated $e^{+}/e^{-}(\lambda_1)$ is much less than the gap length L. Then the number of inverse Compton boosted photons per e^{+}/e^{-} gap traversal is $L/\lambda_1 \gg 1$. When such boosted photons are energetic enough that most are above threshold for making $e^{\pm}$ pairs in the gap on these same soft tertiary photons (mean free path λ_2), the separated charge density in the gap will have an exponentiation length (cf. equation [5.7] of CHR I)

$$h \approx \frac{\lambda_2^2}{2s}\left(\frac{\lambda_1}{L}\right)^2 . \tag{3.10}$$

Since $L \approx s$ and $\lambda_2(\gamma + \text{IR} \rightarrow e^{+} + e^{-})$ is comparable to $\lambda_1(e + \text{IR} \rightarrow e + \gamma)$ for center of mass energy well above the pair production threshold, $h/s \approx (\lambda_1/L)^4 \ll 1$. This short expo-

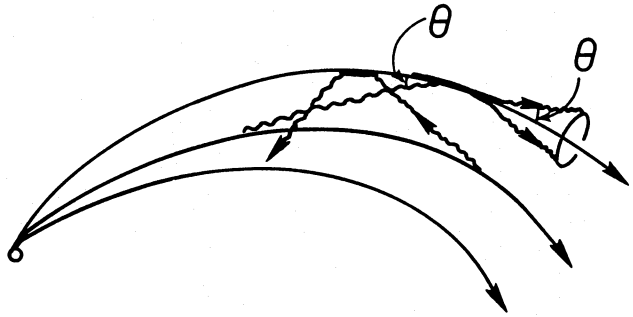

FIG. 2.—Equality between incident γ-ray inclination angle and subsequent synchrotron radiation cone angle for very energetic γ-rays ($E \gg mc^2$) which make pairs in a uniform $\boldsymbol{B}$ field. Secondary γ-ray makes tertiary pairs in (III) and radiates tertiary synchrotron radiation. The outgoing beam is not able to illuminate the gap, while the ingoing beam can.

nentiation path length further supports the assumption made in § V of CHR I on the charge distribution inside the gap.

IV. OUTER GAP RADIATED POWER AND PAIR PRODUCTION

Mechanism (D) of § III in principle allows a self-consistent description of the structure of the outer gap which it controls. However, a reliable quantitative calculation of the steady state of this complicated system is difficult to achieve for several reasons: (1) the structure of the magnetic field heavily loaded with relativistically flowing plasma is not known near the light cylinder; (2) an unknown flow of charge may be sucked into the gap and flow through it from beyond the light cylinder; (3) the seeding rate for gap initiated $e^{\pm}$ showers is not established (and details may depend upon [2]); (4) the gap dynamics cannot be determined by local processes only, since tertiary radiation or primary e^{+}/e^{-} created far away from a particular region of the gap can, nevertheless, dominate the photon and particle density in that region; (5) critical parameters such as gap width and especially $\boldsymbol{B}$ are expected to vary so greatly along the gap length that a single characteristic value can be misleading. We shall, therefore, consider only a qualitative estimate for self-consistent parameters of a dynamic outer gap whose size is assumed to be limited by mechanism (D). We shall apply these to the Vela pulsar and to an extrapolation to other pulsars with different spin rate. (The calculated radiation spectrum of § V is, however, less dependent on these parameters, except for the local magnetic field of the emitting region.)

An outer gap is assumed to have width a, breadth W, and length L along a $\boldsymbol{B}$ field line from its null surface to its light cylinder end. A separated flow F_1 of primary e^{+}/e^{-} passes along $\boldsymbol{B}$ through the gap. These inverse-Compton-scatter on the soft tertiary photons which traverse the gap and give rise to a flux of hard primary γ-rays of magnitude

$$N_1 = F_1 \sigma_T n L \tag{4.1}$$

which extract the power from the gap. Here n is the number density of soft tertiary photons in the gap and σ_T is the Thomson scattering cross section, adequate in this rough estimate because most electron-photon collisions have center of mass energies of $\sim 2mc^2$. Each primary γ-ray escaping the gap is assumed to convert to an $e^{\pm}$ pair in a collision in region (II) with one of the somewhat harder photons found there but not deep in the gap, most of which are radiated before the magnetic mirroring of § V. The creation rate of these secondary $e^{\pm}$ then is

$$F_2 = 2N_1 \, . \tag{4.2}$$

Synchrotron radiation from these secondary pairs is also the source of the flux of secondary γ-rays, X-rays, and soft photons. The rate of synchrotron emission of secondary photons between frequency ω and $\omega + d\omega$ is

$$N_2(\omega)d\omega \approx N_1 \left(\frac{mc^2}{\hbar \omega^{3/2} \omega_B^{1/2}} \right) \gamma_{\parallel}^{1/2} d\omega \, , \tag{4.3}$$

with $\gamma_{\parallel}$ defined for the radiating secondary pairs in equation (5.5) and ω large enough that there is time for the secondary $e^{\pm}$ to radiate to a characteristic peak synchrotron emission ω_c falling below ω. In equation (4.3) F_2 is replaced by N_1 as in equation (4.2). (Even if a significant fraction of these secondary photons pass through the gap, their contribution to the gap n is much less than that from tertiary photons by at least a factor of gap length L divided by λ_1, the mean free path for the inverse Compton scattering of primary e^{-}/e^{+}). The two oppositely directed flux beams of secondary photons pass through each other and make tertiary $e^{\pm}$ pairs. We assume "head on" collisions for the kinematics of a photon of frequency ω from one beam colliding with one of frequency ω' from the crossed beam and approximate the pair production cross section by

$$\sigma = \sigma_P \frac{m^2c^4}{\hbar^2 \omega \omega'} \quad \text{for } \hbar^2 \omega \omega' > m^2c^4 \, , \tag{4.4}$$

and $\sigma = 0$ below the threshold. (The peak pair production cross section $\sigma_P \approx \sigma_T/3$). From equations (4.3) and (4.4), we have an estimate for the rate of tertiary $e^{\pm}$ production:

$$F_3 \approx N_1^2 \gamma_{\parallel}^2 \left(\frac{mc^2}{\hbar \omega_B} \right) \frac{\sigma_P}{W_c} \ln \left(\frac{\omega_{\max}}{\omega_{\min}} \right) . \tag{4.5}$$

(We assume each beam is optically thin to the other, a very good approximation for Vela but not for Crab secondary photons above a GeV.) The origin of the logarithmic factor in equation (4.5) is the (large) range of secondary photon energies in equation (4.3) over which $\omega\omega' > m^2c^4\hbar^{-2}$. The maximum $\hbar\omega \approx$ several GeV, is determined by the maximum primary γ-ray energy (10^{12}–10^{13} eV) to be discussed below. The minimum $\hbar\omega_{\min}$ is the greater of $m^2c^4/\hbar\omega_{\max}$ and the lowest $\hbar\omega$ for which equation (4.3) remains adequate. We shall use the estimate

$$\ln \left(\frac{\omega_{\max}}{\omega_{\min}} \right) \sim \ln \left(\frac{\hbar \omega_{\max}}{mc^2} \right)^2 \approx 20 \, . \tag{4.6}$$

The additional $\gamma_{\parallel}$ factor in equation (4.5) (beyond that from squaring the N_1 of equation [4.3]) comes from the intersection of crossing secondary beams with opening beam angle $1/\gamma_{\parallel}$ when these are assumed to be radiated from a flat emitting surface. As discussed in § V, the synchrotron radiation from those tertiary pairs which move in toward the neutron star irradiate the gap both because of the geometry of $\boldsymbol{B}$-field line convergence and the magnetic mirroring effect which reduces and reflects the pair $v_{\parallel}$. The number density of these soft (generally IR) photons of minimum energy $\hbar\omega_{IR}$ is

$$n \approx \frac{F_3}{WLc} \frac{mc^2}{\hbar \omega_B^{1/2} \omega_{IR}^{1/2}} \, . \tag{4.7}$$

Then from equations (4.7), (4.5), and (4.1) the self-consistency condition for a steady state gap gives a gap tertiary photon density

$$n = \frac{W^2 \hbar^2 \omega_B^{3/2} \omega_{IR}^{1/2}}{F_1^2 \gamma_{\parallel}^2 \sigma_T^2 \sigma_P L m^2 c^2 \ln (\omega_{\max}/\omega_{\min})} \, . \tag{4.8}$$

(Self absorption by the relativistic tertiary $e^{\pm}$ is not important in this estimate for Vela parameters.) The gap must emit primary γ-rays of characteristic energy

$$\hbar\omega_1 \approx m^2c^4/\hbar\omega_{IR} \, , \tag{4.9}$$

since almost all such γ-rays make pairs in the gap and near the gap boundary. Then the total power P_1 transferred from the gap by primary γ-rays into the secondary pairs, and ultimately radiated from the star, is

$$P_1 \approx F_1 \sigma_T n \hbar \omega_1 L \approx \frac{W^2 c^2 \hbar \omega_B}{F_1 \gamma_{\parallel}^2 \sigma_T \sigma_P} \left(\frac{\omega_B}{\omega_{IR}} \right)^{1/2} . \tag{4.10}$$

The geometrical factor $\gamma_{\parallel}^2$ depends on the distance l between the emission of a primary photon in the gap and its conversion to an $e^{\pm}$ pair in the secondary (boundary) region: $\gamma_{\parallel}^2 \approx s^2/l^2$ with s the gap field line radius of curvature. For the model of § V of CHR I, where the main primary emission region is a distance $b \approx a/2$ below the gap boundary, $\gamma_{\parallel}^{-2} = a/s \approx f$, the fraction of the outer magnetosphere occupied by the gap. As discussed in § V of CHR I, models suggest $F_1 \approx fF_1(\max)$ so that $\gamma_{\parallel}^2 F_1 \approx F_1(\max)$ is approximately the total net current through the neutron star polar cap $\sim B_s R^3 \Omega^2 e^{-1} c^{-1}$, with B_s the star's surface dipole field and R the stellar radius (and $B_s R^3$ its magnetic dipole moment). We shall use the conventional estimates for the net polar cap particle flow, and

$$\gamma_{\parallel}^2 F_1 \approx F_1(\max) \approx \begin{cases} 10^{33}\ \mathrm{s}^{-1} & \text{(Vela)}, \quad (4.11a) \\ 10^{34}\ \mathrm{s}^{-1} & \text{(Crab)}. \quad (4.11b) \end{cases}$$

From equation (5.10), with $\tau \approx Lc^{-1}$ and $\gamma_{\parallel} \approx 1$ for the initially inward flowing tertiary pairs (which have smaller $\gamma_{\parallel}$ than that of the secondary ones in eqs. [4.5]–[4.11] and also radiate most efficiently into the gap near their magnetic mirror turnaround points where $\gamma_{\parallel} = 1$),

$$\omega_{\mathrm{IR}} \approx \frac{c^2}{L^2 \omega_B^3} \left(\frac{mc^3}{e^2}\right)^2 \approx \omega_B^{-3} \left(\frac{\Omega mc^3}{e^2}\right)^2 \quad (4.12a)$$

as long as the calculated ω_{IR} exceeds ω_B. Otherwise,

$$\omega_{\mathrm{IR}} \approx \omega_B . \quad (4.12b)$$

(We note from eq. [4.12a] that the number of soft photons radiated per e^+/e^-,

$$\hat{N} \approx \frac{mc^2}{\hbar \omega_B^{1/2} \omega_{\mathrm{IR}}^{1/2}} \approx \frac{e^2}{\hbar c} \omega_B \frac{L}{c},$$

is also the same as the number from an e^+/e^- whose characteristic synchrotron radiation frequency $\omega \approx \gamma_{\parallel} \gamma_{\perp}^2 \omega_B$ is already less than the ω_{IR} of eq. [4.12a]. Therefore eq. [4.7] with eq. [4.12a] includes both contributions.)

For Vela, near its light cylinder $\omega_B \ll 3 \times 10^{12}\ \mathrm{s}^{-1}$, and equation (4.12a) is appropriate. For the Crab, with ω_B about 27 times greater, equation (4.12b) should be used. From equations (4.10)–(4.12) we then have for the radiated power of a Vela outer gap

$$P_1 \approx \frac{LW^2 e^2 \hbar \omega_B^3}{F_1(\max) \sigma_{\mathrm{T}} \sigma_P mc^2 \ln(\omega_{\max}/\omega_{\min})}, \quad (4.13a)$$

and, for a Vela-type outer gap with Crab-like parameters,

$$P_1 \approx \frac{W^2 c^2 \hbar \omega_B}{F_1(\max) \sigma_{\mathrm{T}} \sigma_P mc^2 \ln(\omega_{\max}/\omega_{\min})}. \quad (4.13b)$$

Although the essentially dimensional estimates given in equations (4.13a)–(4.13b) can hardly be quantitatively reliable, we give some numerical evaluation of them below. A similar kind of estimate for total energy loss would lead to $\dot{E} \approx B^2 W^2 c \approx 3 \times 10^{36}$ ergs s^{-1} and to a total current $eF_1(\max) \approx e\Omega B W^2 \approx 10^{33} e\ \mathrm{s}^{-1}$. These are reasonable but only because of a particular and rather arbitrary dropping of numerical factors like 2π which could, even more plausibly, have been included in the estimate. These estimates may, however, correctly exhibit the dependence of P_1 on pulsar parameters and do give an indication of its approximate order of magnitude which, for Vela, is similar to that of the total pulsar power.

If the gap were controlled only by local pair production and photon radiation, the power could also vary greatly along the gap, with a greater γ-ray power expected from regions nearer the star where B is larger in Vela-type pulsars, since $W^2 \omega_B^3 \propto \Phi_B B^2$, i.e., to B^2. The geometrical interpretation of the observed 140° pulse interpulse separation of § IV of CHR I implies that our line of sight to the Crab and Vela pulsars is sufficiently inclined with respect to their spin axes that we observe secondary radiation emitted from nearer the light cylinder. We shall, therefore, evaluate P_1 of equations (4.13a) and (4.13b) with light cylinder parameters. For Vela with $W \approx L \approx 5 \times 10^8$ cm, and a gap-averaged magnetic field $\bar{B} \approx B_s(R/L)^3 \sim 2 \times 10^4$ G, $\omega_B \approx 3 \times 10^{11}\ \mathrm{s}^{-1}$, $F_1(\max) \approx 10^{33}\ \mathrm{s}^{-1}$, and equation (4.6), we have

$$P_1(\mathrm{Vela}) \approx 3 \times 10^{35}\ \mathrm{ergs\ s}^{-1} \approx 3 \times 10^{-2} I \Omega \dot{\Omega}. \quad (4.14)$$

The observed P_1(Vela), if interpreted as a fan beam, is about 10^{35} ergs s^{-1}. The Vela total spindown power is $\sim 10^{37}$ ergs s^{-1}, so the gap power is several percent of the total spindown power. Such a gap would have to have a thickness $\gtrsim \frac{1}{3}$ that of a completely evacuated outer magnetosphere. The crude model result for total tertiary pair production in Vela is

$$F_3(\mathrm{Vela}) \approx \left(\frac{\hbar c}{e^2}\right) \frac{W^3 c^3 \hbar}{F_1(\max) F_1 \sigma_{\mathrm{T}}^2 \sigma_P m L^2 \omega_B \ln(\omega_{\max}/\omega_{\min})} \approx 10^{37}\ \mathrm{s}^{-1}. \quad (4.15)$$

[A more quantitative estimate given in §VIII*c* gives $F_3(\mathrm{Vela}) \approx 10^{36}\ \mathrm{s}^{-1}$.] Such a particle flux (if these particles are further accelerated beyond the Vela light cylinder) is more than adequate to support the observed synchrotron X-ray nebula around Vela. The power of a Vela-type outer gap with Crab-like parameters from equation (4.13b) with $W = 1.5 \times 10^8$ cm, $\omega_B = 10^{13}\ \mathrm{s}^{-1}$, $F_1(\max) = 10^{34}\ \mathrm{s}^{-1}$, and $\ln(\omega_{\max}/\omega_{\min})$ from equation (4.6) is

$$P_1(\mathrm{Crab}) \approx 10^{37}\ \mathrm{ergs\ s}^{-1} \approx 10^{-2} I \Omega \dot{\Omega}, \quad (4.16)$$

about 30 times the predicted power from the Vela model and about an order of magnitude larger than the total observed power in the Crab pulse plus interpulse if they are interpreted as fan beams. (However, details of the Crab outer gap control mechanism should include the absorption of secondaries of energy >GeV by crossed secondary beam X-rays, an absorption which is negligible for Vela.) The predicted tertiary pair production rate in the Crab outer magnetosphere is

$$F_3(\mathrm{Crab}) \approx \left(\frac{\hbar \omega_B}{mc^2}\right)^3 \frac{W^3 c^3}{F_1(\max) F_1 \sigma_{\mathrm{T}}^2 \sigma_P \ln(\omega_{\max}/\omega_{\min})} \approx 10^{38}\ \mathrm{s}^{-1}, \quad (4.17)$$

for $F_1/F_1(\max) \approx 0.2$ to give the result of equation (4.16). This is about the rate of $e^{\pm}$ pair injection needed to give the observed Crab nebula emission (Kennel and Coroniti 1984).

Model outer gap–related rough estimates for Vela are given below with their dependence on the near light cylinder averaged magnetic field $\bar{B}$:

$$\Delta V_0 \approx 10^{15} \bar{B}_4\ \mathrm{V},$$

$$\omega_{\mathrm{IR}} \approx 10^{15} \bar{B}_4^{-3}\ \mathrm{s}^{-1},$$

$$\text{average primary } \gamma\text{-ray energy} \approx 10^{12} \bar{B}_4^3\ \mathrm{eV},$$

$$\lambda = \text{mean free path of primary } e^{\pm} \approx 10^{-3} \bar{B}_4^2 L,$$

$$n \approx 10^{18} \bar{B}_4^{-2}\ \mathrm{cm}^{-3},$$

$$F_3 \approx 10^{37} \bar{B}_4^{-3}\ \mathrm{s}^{-1}.$$

The average primary e^+/e^- energy in the gap is $e\Delta V_0\,\lambda/L$, so that

$$\gamma_1 \approx 10^6 \bar{B}_4^3 .$$

The model IR radiation luminosity

$$L_{\rm IR} \approx n\hbar\omega_{\rm IR}\, cWL \sim 10^{33}\bar{B}_4^{-5}\ {\rm ergs\ s^{-1}} .$$

For $\bar{B}_4 > 1$, the Vela model IR luminosity would not have been an *IRAS* source. Based on the above, we shall take for our model Vela gap in § V $\bar{B}_4 \approx 2$, so that $\omega_{\rm IR} \approx 0.1$ eV. The ratio of the Vela outer gap model primary emission power by curvature radiation to that by inverse Compton scattering is

$$\frac{\gamma_1^4 e^2 \lambda_1}{s\gamma_1 mc^2 L} \approx 10^{-8} B_4^{11} , \tag{4.18}$$

so that for Vela, parameter curvature radiation is expected to be negligible. However, the ratio rises sharply with decreasing period (Ω^{27}), so that for pulsars with Crab-like parameters mechanism (3) may dominate.

For Vela-like pulsars and observation angles, except for different spin rate Ω and surface dipole component B_s, the estimates of this section scale as follows: f is independent of B_s and Ω, and

$$P_1 \propto B_s^2 \Omega^4 , \tag{4.19}$$

$$F_1 \propto B_s \Omega^2 , \tag{4.20}$$

$$\omega_{\rm IR}\,({\rm if} > \omega_B) \propto B_s^{-3}\Omega^{-7} , \tag{4.21}$$

$$\text{energy of the primary } \gamma\text{-ray (if } \omega_{\rm IR} > \omega_B) \propto B_s^3 \Omega^7 , \tag{4.22}$$

and

$$\lambda/L \propto B_s^2 \Omega^5 . \tag{4.23}$$

With increasing Ω the ratio $\omega_{\rm IR}/\omega_B$, which is around 10^3 for Vela with $B_4 \approx 2$, falls like $B_s^{-4}\Omega^{-10}$. Therefore, for a pulsar with $B_s^{4/10}\Omega$ more than $10^{3/10} \approx 2$ times greater than that of Vela, the estimate of equation (4.12a) must be replaced by equation (4.12b): for a Vela-type outer gap with Crab-like parameters, the power and volume of the gap begin to decrease relative to their maxima if they filled the outer magnetosphere. Equations (4.19)–(4.23) are then replaced by

$$P_1 \propto \Omega^{-1} , \tag{4.19'}$$

$$F_1 \propto B_s^{1/3}\Omega^{1/3} , \tag{4.20'}$$

$$\omega_{\rm IR} = \omega_B \propto B_s \Omega^3 , \tag{4.21'}$$

$$\text{energy of the primary } \gamma\text{-ray} \propto B_s^{-1}\Omega^{-3} , \tag{4.22'}$$

$$\lambda/L \propto B_s^{2/3}\Omega^{5/3} , \tag{4.23'}$$

and for the fraction f of available volume occupied by the outer gap,

$$f \propto B_s^{-2/3}\Omega^{-5/3} . \tag{4.24}$$

A Vela-type model outer gap for the millisecond pulsar PSR 1937+214 with an implied $B_s\Omega^2$ about the same as that of Vela should then be described by equations (4.19')–(4.23') and (4.24). It would have much more energetic primary γ-rays emitted from it than an outer gap with Crab-like parameters, but its total power output would be much less than that from the Vela. Consequences for the observable secondary radiation will be discussed elsewhere.

If the maximum secondary synchrotron photon energy falls below mc^2, tertiary pairs will no longer be created in our Vela-type gap approximation. For the Vela-type estimates above this will occur when $[B_s/B_s({\rm Vela})]^7[\Omega/\Omega({\rm Vela})]^{17} \approx 10^{-3}$, so that the gap power is $10^{-12/17}P_1({\rm Vela}) \approx 0.2P_1({\rm Vela}) \approx 2 \times 10^{34}$ ergs s^{-1}. For lower Ω the above scaling fails, as the fraction of the outer magnetosphere occupied by the gap (independent of Ω in the model estimate) increases from about $\frac{1}{3}$ toward unity. Outer gap switching from a self-sustained discharge to an "amplifier gap" (Cheng, Ruderman and Sutherland 1976) occurs when essentially all the available pulsar spindown power is used in maintaining the needed outer gap power. In this transition regime, gap power drops much more slowly with Ω than indicated in equation (4.19), so that steady self-sustained outer gaps would be expected to turn off when the total pulsar power spindown energy falls below about 10^{34} ergs s^{-1}.

In summary, an outer gap controlled by a Vela-type pair production process has a ratio of radiated power to $I\Omega\dot{\Omega} \approx 10^{-2}$, which is independent of P and B_s when both parameters are near those of Vela. This ratio becomes proportional to $\eta \equiv B_s^{-2}P^5$ when η falls below much less than $10^{3/2}$ that of Vela and rises to unity for $\eta \approx 10^2$ that of Vela.

V. VELA PULSAR SPECTRUM: OPTICAL–GeV

a) X-Rays and γ-Rays

In our model for a young pulsar's dynamic outer gap, the observed double fan-beamed radiation comes from just beyond the upper gap boundary (region [II] of Fig. 1). This region is optically thick to pair creation by primary inverse Compton γ-rays whose energy extends to 10^4 GeV. The resulting spectrum of synchrotron radiation by the secondaries produced there depends on gap parameters which determine the primary spectrum and on the local magnetic field of the observed part of the secondary emission region. The model gap parameters, such as particle flow through the gap F_1, gap IR photon density n, and spectrum, are globally determined if the dynamics of different gap stretches are independent. However, in considering the observable gap-powered secondary photon spectrum, the position of the gap boundary emission region which is being observed (cf. § IV of CHR I) has a particularly important effect in determining certain key emission parameters. The upper and lower extremes of the radiated energy spectrum (<1 KeV and >1 GeV), in particular, are especially sensitive to the local gap magnetic field which, in the dipole approximation, decreases as the cube of the distance from the emission region to the star. As indicated in Figure 9 of CHR I, the measured 140° separation between pulse and interpulse in the Vela and the Crab pulsars indicates that for a rigidly corotating outer magnetosphere the emission regions being observed would be ~0.6 the light cylinder distance away from the pulsar spin axis. The distance between that region and the star also depends upon the unmeasured angle χ between the pulsar's dipole moment and spin axis. For large χ it may be very considerably larger than its distance to the spin axis. When the latter is already comparable to the light cylinder radius, as is the case here, the emission region can be even more distant from the neutron star than the light cylinder radius $c\Omega^{-1}$. Its local B, which depends sensitively on that distance in the dipole approximation, can be considerably less than the near light cylinder average B which was used in § IV to estimate gap properties. (For $\bar{B}$ the most important region was expected to be near the magnetic mirror bounce for inward

moving pairs, where the local $\boldsymbol{B}$ is typically about twice that of the place where the pairs were created.)

In calculating the secondary synchrotron spectrum for Vela-type pulsars we adopt the following relevant gap and local $\boldsymbol{B}$ parameters: (1) A soft tertiary radiation intensity spectrum flowing through the secondary and gap regions (cf. eq. [2.16])

$$I_3 = \begin{cases} \text{constant}\,, & \omega_0 < \omega \leq \omega_{\rm IR}\,, \\ 0\,, & \omega > \omega_{\rm IR} \end{cases}, \tag{5.1}$$

with

$$\omega_{\rm IR} \approx 10^{-1}\ \text{eV} \tag{5.2}$$

from $\bar{B} \approx 2 \times 10^4$ G in § IV (eq. [4.14]). The much lower $\omega_0 \ll \omega_{\rm IR}$ self-absorption limit is not quantitatively significant here and will be neglected. (2) A maximum primary γ-ray energy

$$E_1(\gamma) \approx 10^7\ \text{MeV}\,, \tag{5.3}$$

to give a center of mass energy in collisions with the most energetic soft photons of the spectrum of equation (5.1) sufficient to make $e^{\pm}$ pairs:

$$E_{\rm CM} \approx \sqrt{2\hbar\omega_{\rm IR} E_\gamma} \approx 2\ \text{MeV}\,. \tag{5.4}$$

In equation (5.4) it is assumed that the tertiary soft photon and primary photon momenta are typically perpendicular and that the CM energy is about twice threshold (where the pair production cross section becomes large). A more realistic description of the primary γ-ray flux would have a broader, correlated distribution for ω and $\gamma_\parallel$, but our general results are not sensitive to these details. We approximate the intensity spectrum of the primary photons from the inverse Compton boosting of the soft photon spectrum of equation (5.1) by a constant

$$I_1(\omega) = A \tag{5.6a}$$

for $E_1\,\omega_0/\omega_{\rm IR} < \hbar\omega < E_1 = 10^7$ MeV, and

$$I_1(\omega) = 0 \tag{5.6b}$$

outside this range. (This approximation ignores the reduction in the inverse Compton cross section for primary e^+/e^- on the soft tertiary photons in the gap from $\sigma_{\rm T}$, its value as long as $E_{\rm CM} \ll mc^2$, to a value nearer to σ_P at the upper end of the spectrum where $E_{\rm CM} \gtrsim mc^2$.) The secondary $e^{\pm}$ pairs, flowing along $\boldsymbol{B}$ in both directions with the same $\gamma_\parallel$ as the incident primary γ-ray which created them, will have a uniform distribution in γ from a maximum $\gamma \approx E_1/2mc^2 \approx 10^7$ down to $10^7\omega_0/\omega_{\rm IR}$. The resulting synchrotron photon number intensity in each crossed secondary beam is then, to good approximation,

$$N_2(\omega) \propto \omega^{-3/2} \ln\left(\frac{\omega_{\rm max}}{\omega}\right), \tag{5.7}$$

with

$$\hbar\omega_{\rm max} = \left(\frac{E_1}{2mc^2}\right)^2 \frac{\hbar\omega_B}{\gamma_\parallel} \sim 3 \times 10^9\ \text{eV}\,. \tag{5.8}$$

Equation (5.7) assumes that the synchrotron-radiating secondaries remain in the relevant part of the magnetosphere long enough to permit their initial $\gamma_\perp$ to fall to a $\hat{\gamma}_\perp$ such that $\omega_c = \hat{\gamma}_\perp^2 \gamma_\parallel \omega_B < \omega$. For Vela geometry and the assumed local $\boldsymbol{B}$ cutoff, the secondary spectrum of equation (5.7) has a break at $\hbar\omega = \hbar\omega_c(2) > 10$ KeV. For equation (3.4), a break in the observed secondary spectrum will occur at

$$\omega = \omega_c \approx \frac{\gamma_\parallel^3}{\omega_B^3}\left(\frac{e^2}{mc^3}\right)^2\left(\frac{c}{\kappa L}\right)^2, \tag{5.9}$$

where κ is the fraction of the gap length traversed by a secondary e^-/e^+ before it reaches the observed emission region, which we shall take to be near the middle of the outer gap's secondary region. Then (see Fig. 3), for a field line segment whose length equals its curvature radius, $\gamma_\parallel^3/\kappa^2 = \kappa^{-2}(1/2 - \kappa)^{-3}$, which has a minimum value (at $\kappa = \frac{1}{5}$) of 926. For $L \approx 6 \times 10^8$ cm and $B \approx 5 \times 10^3$ G, the minimum achievable $\hbar\omega_c$ in (equation (5.9) is

$$\omega_c \approx \frac{10^3}{\omega_B^3}\left(\frac{e^3}{mc^3}\right)\left(\frac{c}{L}\right)^2 \approx 25\ \text{KeV}\,. \tag{5.10}$$

For secondaries with other than optimal $\gamma_\parallel$, which gives equation (5.11), ω_c' is greater. For $\omega < \omega_c' \approx 10^2$ KeV, we approximate

$$N_2(\omega) \approx N_2(\omega_c')\left(\frac{\omega}{\omega_c'}\right)^{-2/3}, \tag{5.11}$$

since $I(\omega) \propto (\omega/\omega_c)^{1/3}$ for $\omega \ll \omega_c$. The numerically integrated synchrotron photon spectrum (to which eqs. [5.11] and [5.7] are only an approximation), normalized to carry the same integrated intensity as the observed one, is compared to observations in Figure 4. The best power-law fit ($\omega^{-\nu}$) to the observed γ-ray data above 50 MeV (Kanbach *et al.* 1980) has

$$\nu = \begin{cases} 1.77 \pm 0.15\,, & (50\text{–}300\ \text{MeV})\,, \\ 2.0 \pm 0.2\,, & (300\text{–}3000\ \text{MeV})\,, \end{cases} \tag{5.12}$$

while equation (5.7) gives $\nu = 3/2 + [\ln(\omega_{\rm max}/\omega)]^{-1}$ or

$$\nu = \begin{cases} 1.85\,, & (175\ \text{MeV})\,, \\ 2.22\,, & (750\ \text{MeV})\,, \end{cases} \tag{5.13}$$

From equation (5.10), the value of $\gamma_\parallel$ at the spectral break is $\gamma_\parallel \approx (1/2 - \kappa)^{-1} \approx 10/3$, corresponding to a minimum half-width for the peak of Vela's (unmeasured) X-ray spectrum of $\sim$5 ms. We note that the model secondary synchrotron radiation falls two orders of magnitude below the observed optical radiation. That radiation has another origin (tertiary radiation from deeper in the magnetosphere), which will be discussed next.

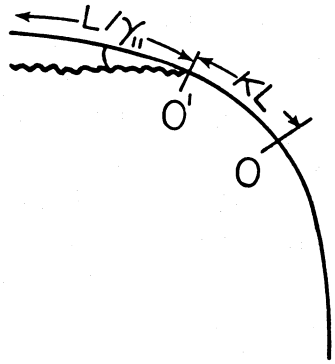

FIG. 3.— A primary γ-ray makes and $e^{\pm}$ pair at O' a distance at least $L/\gamma_\parallel$ beyond the null surface point on the field line $\boldsymbol{B}$. Synchrotron radiation from the pair is observed at O a distance κL beyond O'.

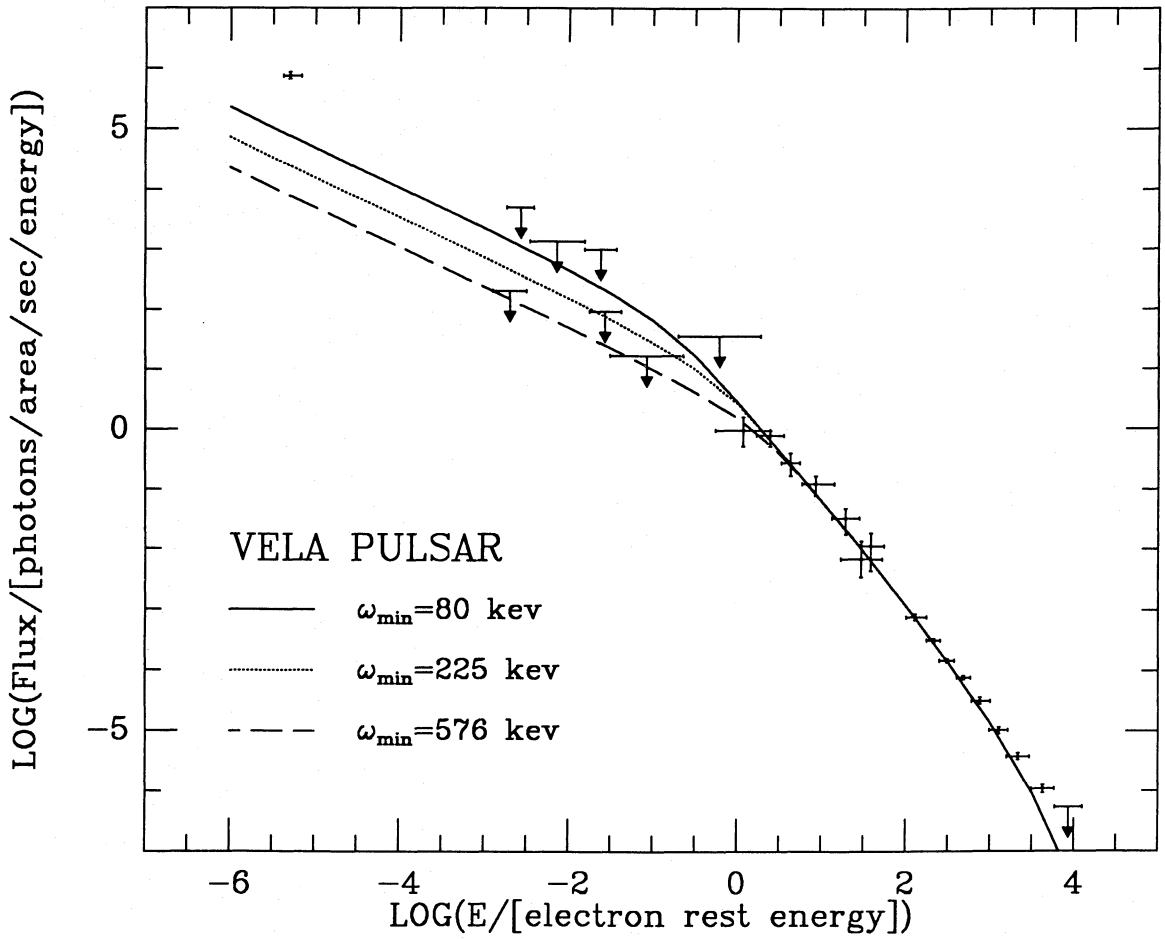

FIG. 4.—Calculated and observed spectra of the pulsed electromagnetic emission from the Vela pulsar. The theoretical spectra use the parameters discussed in § V: emission region magnetic field $B = 5 \times 10^3$ G, $\hbar\omega_{max} = 3$ GeV. The solid, dotted, and dashed lines use ω_{min} as 80, 225, and 576 keV respectively. The spectra are normalized to fit the observed γ-ray intensity. (Observed data are taken from Albats, Frye, and Thomson 1974; Kanbach *et al.* 1980; Knight *et al.* 1982; Tümer *et al.* 1984; Harnden *et al.* 1985.) The theoretical curve for modulated X-rays around 1 keV does not include an expected contribution between pulses from thermal polar cap emission. Its inclusion would raise observationally derived upper limit by diminishing the amount of modulation. (cf. § VIIIe).

b) Optical

As discussed earlier, synchrotron radiation from those secondaries which are the source of Vela's γ-rays is insufficient to give even its weak observed optical power. However, the synchrotron radiation from tertiary pairs, especially the inward flowing ones as they are reflected by the converging magnetic field, can also radiate optical photons with the same declination angle relative to the pulsar's spin axis as that of the observed γ-rays (cf. Fig. 5). We have already seen in the previous discussion that $B \approx 5 \times 10^3$ G in the local region from which the observed X-ray and γ-ray beams are emitted. The outer magnetosphere region (III) which is the source of the soft photons in the gap is expected to be somewhat closer to the star, both because it is determined by the mirroring positions of the inward-flowing pairs and also because more synchrotron power is radiated when B is larger. In §§ III and IV, the B for tertiary radiation which gave the gap $\hbar\omega_c \approx 10^{-1}$ eV was $B \approx 2 \times 10^4$ G. The relation of distances to the star of the relevant observed tertiary and secondary regions would then be

$$\left(\frac{r_3}{r_2}\right) \approx \left(\frac{B}{\bar{B}}\right)^{1/3} \approx (4)^{-1/3} . \qquad (5.14)$$

The geometrical arguments of CHR I lead to an observed interval between the main pulse and interpulse roughly proportional to the distance between the emission regions and the rotation axis. Then the expected phase separation of Vela's (tertiary) optical pulses ($\Delta\psi_{opt}$) relative to that of its secondary

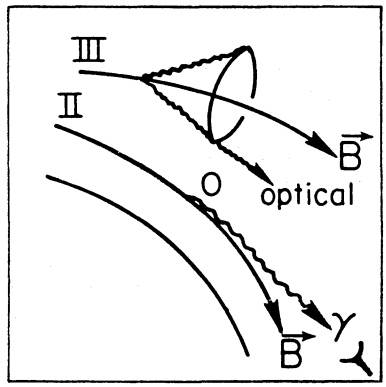

FIG. 5.—Optical and γ-ray radiating regions in the outer magnetosphere of the Vela pulsar.

X-ray and γ-ray ones ($\Delta\psi_\gamma$) would be

$$\Delta\psi_{\rm opt} \approx \left(\frac{r_3}{r_2}\right)\Delta\psi_\gamma \approx \frac{140^\circ}{\sqrt[3]{4}} \approx 90^\circ , \quad (5.15)$$

in agreement with the observation. As shown in CHR I, the midpoint between these optical pulses should (and does) coincide with that of the γ-ray pulses. The total optical luminosity from the relevant tertiary region comes mainly from the synchrotron radiation of those tertiary $e^\pm$ whose initial $\gamma \equiv E/mc^2$ satisfies $\gamma_\parallel \gamma_\perp^2 \hbar\omega_B \approx 2\gamma^2 \times 10^{-4}$ eV > 2 eV. These $e^\pm$ pairs must have been created by secondary γ-rays with $\hbar\omega = 2\gamma mc^2 > 10^2$ MeV, and these mainly materialize as pairs on crossed-beam X-ray photons of energy less than 10 KeV, below the spectral break of equations (5.9) and (5.10) and Fig. 4. The main contributor to optical radiation ($\hbar\omega = 2$–8 eV) comes from those tertiary $e^\pm$ whose γ are in the range 1–2×10^2. Thus the total radiated optical power is $\sim 10^{-4}$ ergs times the creation rate of the tertiary $e^\pm$ whose initial energy exceeds 10^2 MeV, $F_3(>10^2$ MeV). With $I_2(\omega)$, the secondary (and observed) beam intensity and the $e^\pm$ pair production cross section approximated by equation (4.4) is

$$F_3(>10^2 \text{ MeV}) \sim 4 \int_{(m^2c^4/3\text{ GeV})}^{(m^2c^4/10^2\text{ MeV})} d\omega' \frac{I_2(\omega')}{\hbar\omega'} \int_{(m^2c^4/\hbar\omega')}^{3\text{ Gev}} d\omega \times \left(\frac{I_2(\omega)}{\hbar\omega}\right)\left(\frac{m^2c^4}{\hbar^2\omega\omega'}\right)\left(\frac{\sigma_P L}{Wc}\right) . \quad (5.16)$$

In the ω integration region (3 GeV $> \hbar\omega > 10^2$ MeV), we approximate the $I_2(\omega)$ of equation (5.7) (and that observed) by an appropriately normalized power law:

$$I_2(\omega) \approx \frac{2 \times 10^{35} \text{ ergs s}^{-1}}{\omega \ln (3 \text{ GeV}/30 \text{ MeV})} . \quad (5.17)$$

Then the optical luminosity becomes

$$L_{\rm opt} \approx \frac{2\sigma_P}{Wc} \frac{4 \times 10^{34} \text{ ergs s}^{-1}}{m^2c^4} \int_{10^2\text{ eV}}^{2.4\text{ KeV}} d\omega' I_2(\omega') . \quad (5.18)$$

The integrated intensity is over an interval where only an upper bound is available. From the model equations (5.7) and (5.11) and Fig 4, we estimate the integral in equation (5.18) as $\sim 10^{32}$ ergs s^{-1}. With $\sigma_P \approx 2 \times 10^{-26}$ cm^2 and $W \approx 5 \times 10^8$ cm, equation (5.18) then gives

$$L_{\rm opt} \approx 10^{30} \text{ ergs s}^{-1} , \quad (5.19)$$

which does not conflict substantially with the optical observation for an assumed fan beaming. We note also that because the tertiary pairs have $\gamma_\parallel \approx 1$ at mirroring and this value is quite generally considerably less than that of the synchrotron radiating secondaries, tertiary radiation cannot be as narrowly beamed as is secondary radiation. This is supported by the broader width of Vela's optical pulses than that of its γ-ray pulses.

For the Crab pulsar, $\omega_B^3 L^2$ in equation (5.9) is larger than its value in Vela by over 10^3, so that $\hbar\omega_c \lesssim 10^2$ eV, and the Crab pulsar's strong optical radiation can be attributed to secondary synchrotron radiation from the same $e^\pm$ as those that give its observed X-rays. However, we cannot simply apply the spectrum of equations (5.7) and (5.12) to the Crab for two reasons. Secondary GeV γ-rays will be largely absorbed by keV secondary X-rays in the crossed beam. This and subsequent inverse Compton scattering of secondary pairs would alter its spectrum, mainly by increasing its X-ray intensity at the expense of its high-energy γ-ray intensity. However, more importantly. before the Crab pulsar's gap can grow large enough for the mechanisms in § IV to limit it, $e^\pm$ production mechanism (C) of § III becomes dominant. This will be discussed in the next section.

VI. CRAB OUTER GAP RADIATED POWER AND PAIR PRODUCTION

The control mechanism for the Crab is less transparent than that for Vela. Because of the smaller radius of curvature (eq. [4.18]) and a smaller gap flux of photons from mirrored tertiary pairs (§ III), curvature radiation competes much more favorably with inverse Compton scattering in the gap as a means of taking energy out of energetic primary e^+/e^-. Moreover, the soft X-ray intensity from the Crab (both that calculated for the mechanisms and that which is observed), would result in the complete conversion of such GeV γ-rays into $e^\pm$ as they pass through a secondary beam. Although the curved field line geometry constrains the collimated secondary X-rays (§ III), and only a small fraction of them can penetrate deeply into the gap, because of the large $N_\gamma(\sim \gamma_1 e^2/\hbar c \approx 10^5)$, the charge exponentiation length h of equation (5.7) in CHR I can be sufficiently small to sustain efficient gap pair production: primary curvature radiation γ-rays from gap-accelerated primary e^+/e^- convert to $e^\pm$ pairs on the synchrotron X-ray radiation from the $e^\pm$ which the primary radiation makes just beyond the gap. We consider below the (minimum) needed power and the dependence on B_s and Ω of a "Crab-like" outer gap controlled this way (mechanism [C] of § II).

Primary curvature γ-rays from e^+/e^- with $\gamma_1 \equiv E_p/mc^2$ have a characteristic energy

$$\hbar\omega_1 = \gamma_1^3 \hbar c/s . \quad (6.1)$$

To create synchrotron secondary radiation whose photon energy is sufficiently large that collisions of secondary photons with primaries can have the center of mass energy above $2mc^2$ needed for pair creation, a necessary condition is

$$\gamma_\parallel^{-1}(\gamma\hbar/mcs)^3 \hbar\omega_B > mc^2 . \quad (6.2)$$

An outer gap whose length $L \approx s$ must then have a maximum total potential drop along L of

$$\Delta V \approx \frac{e\gamma_1^4}{s} > \left(\frac{\gamma_\parallel mc^2}{\hbar\omega_B}\right)^{4/9}\left(\frac{mcs}{\hbar}\right)^{4/3}\frac{e}{s} . \quad (6.3)$$

For a Crab $B \approx 2 \times 10^5$ G, larger than that used for Vela by about a ratio of their Ω^3, $s = 10^8$ cm, and $\gamma_\parallel \approx 3$,

$$\Delta V > 10^{14} \text{ V} . \quad (6.4)$$

If the Crab outer gap can be limited in this way to the minimum potential drop equation (6.4), then the limited gap width is only a fraction, $f \approx 5 \times 10^{-2}$, of the maximum that could be achieved by a gap which fills the available open magnetosphere ($\Delta V \propto f^2$ and $\sim 4 \times 10^{16}$ V) at $f \approx 1$. The so limited outer gap particle flux $F_1 \approx 10^{33}$ s^{-1}, and the gap-radiated power

$$P_1 \approx e\Delta V \times 10^{33} \text{ s}^{-1} = 2 \times 10^{35} \text{ ergs s}^{-1} . \quad (6.5)$$

This is several times less than that actually observed to be emitted from the Crab pulsar if radiated fan beams are assumed. The estimated power of equation (6.5), and the frac-

tion gap width ($f \approx 10^{-1}$) needed to achieve it, are less than the estimates of these quantities from the Vela-type control mechanism of § IV. It is, however, difficult to conclude with confidence that the "Crab-type" control of an outer gap which is considered here would necessarily be effective before the gap grows large enough for the Vela-type control of § IV to dominate. Secondary X-ray photons would be needed deep within the gap for pair conversion by the GeV curvature primaries. However, how deeply secondaries penetrate into the gap is not easy to determine, since the plasma-loaded boundary $\boldsymbol{B}$-field shape is uncertain near the light cylinder. (This is not a problem for the tertiary IR radiation from magnetic mirroring tertiary pairs penetrating into a Vela-type gap.) On the other hand, for the reasons discussed in § II, although a Vela pulsar outer gap would not be limited the presumed Crab-type control mechanism, a Crab pulsar outer gap must have much of its power extracted by curvature radiation (cf. eqs. [4.18] and following). For a Crab-type outer gap, the (minimum) ratio of gap width to the maximum width according to the criterion of equation (6.2) (which is a necessary but not sufficient condition for a Crab-type gap) is

$$f \approx \left(\frac{B_q}{B}\right)^{13/20} \left(\frac{e^2}{\hbar c}\right)^{9/20} \left(\frac{\hbar}{mcs}\right)^{3/10} , \qquad (6.6)$$

where B is the average outer gap mangetic field and $B_q \equiv m^2c^3/e\hbar = 4.4 \times 10^{13}$ G. For $s \approx c/\Omega$, $B = B_s R_s^3 s^{-3}$, and $R_s = 10^6$ cm, the minimum power P_1 needed of an outer gap controlled by a Crab-type mechanism satisfies

$$\frac{P_1}{I\Omega\dot{\Omega}} \approx f^3 \approx 10^{-4} \left(\frac{3 \times 10^{12}\ \mathrm{G}}{B_s}\right)^{39/20} \left(\frac{P}{0.03\ \mathrm{s}}\right)^{99/20} . \qquad (6.7)$$

We consider the spectrum of the secondary emission associated with such a gap in the next section.

A gap might also consist of various regions which at different stretches and depths are controlled by mechanism (C) and (D). For regions controlled by mechanism (C), the analysis in this section may be appropriate. For regions controlled by mechanism (D), the discussion in § IV with Crab parameters should be used. The analysis of the interdependence between these regions and field line structure is complicated and beyond the scope of this paper.

VII. CRAB PULSAR SPECTRUM: OPTICAL–GeV

Even though the particular controlling mechanism for a Crab outer gap may be rather sensitive to uncertain outer magnetosphere parameters, the resulting secondary emission spectrum can be considered with greater confidence because of the emission geometry. For crossed beam emission like that described in Figure 7 of CHR I, a beam of photons crosses an oppositely directed beam of photons which is an almost identical mirror image of itself before reaching the observer. Such crossing energetic photon beams result in additional pair production, which modifies the emitting particle distribution. The tertiary e^+/e^- considered in § III for Vela is such an example, but the beam optical depths for γ-ray absorption and conversion were small. However, for the Crab, because of the similarity in the energy range and because of stronger beam-beam absorption, the distinction between the secondary and tertiary is not as useful for the Crab as for Vela, and we shall no longer make it.

We use the observed pulsed X-ray emission from the Crab (which is certainly emitted from the same place as the γ-ray and optical pulses) as an input to our modeling of the Crab's secondary particle distribution and complete spectrum. A test of self-consistency for the model is the comparison of the calculated and the observed spectrum. Secondary photons affect secondary pairs and their emission in two ways. First, they will collide with each other and convert into $e^{\pm}$ pairs when the collision CM energy is above the pair creation threshold. As discussed in § VI, some of the secondary photons may return into the gap and provide target X-ray photons which collide with primary curvature γ-rays and sustain the primary charge exponentiation there. They are certainly more copious in the secondary region, and most of the primary γ-rays (either GeV or curvature γ-rays or 10^{12} eV inverse Compton boosted γ-rays) will be converted. Since photons with different energies convert with different mean free paths, the particles will be spatially distributed according to the conversion probability, which is a function of their energies. Second, the secondary photons can inverse Compton scatter with the same secondary relativistic $e^{\pm}$'s whose synchrotron radiation is their source and take energy away from them. For Crab parameters and secondary beam intensities, the inverse Compton scattering emission power of the secondaries can be comparable to their synchrotron radiation. Because of these two effects, the initial secondary particle distribution from the conversion of primaries is less crucial in determining the final emitted spectrum, and the uncertainty in deciding the role of different possible gap-controlling mechanisms becomes less important.

The Crab pulsar's pulsed spectrum is well measured in optical regimes and from keV to GeV. The similar timing of the subpulses from frequencies different by orders of magnitude implies the same emission areas. Thus the observed flux can be translated into the photon number density in the emission region. The secondary photon number density as a function of energy can be approximated by the piecewise (continuous) power law $n(\omega) \propto \omega^{\nu(\omega)}$ (see Fig. 6), where $\nu(\omega)$ is given by

$$\nu(\omega) \approx \begin{cases} -2.2 , & \hbar\omega/mc^2 \gtrsim 1 , \\ -1.8 , & 1 \gtrsim \hbar\omega/mc^2 \gtrsim 3 \times 10^{-3} , \\ -1.25 , & 3 \times 10^{-3} \gtrsim \hbar\omega/mc^2 \gtrsim 3 \times 10^{-6} , \\ -0.66 , & 3 \times 10^{-6} \gtrsim \hbar\omega/mc^2 . \end{cases} \qquad (7.1)$$

The absolute MeV photon density based on the observed absolute intensity of the Crab pulsar at a distance of 2 kpc is

$$n(\hbar\omega \approx mc^2) \approx 10^{15} A_{16}^{-1}\ \mathrm{cm}^{-3} , \qquad (7.2)$$

where A_{16} is the emission area in units of 10^{16} cm^2, and other photon energy regime densities are related to that of equation (7.2) by equation (7.1). In passing through this screen of secondary photons, essentially all the primary photons with energy greater than a few GeV are converted into secondary $e^{\pm}$'s.

A recipe for calculating the secondary emission spectrum is given in the Appendix (after Ho 1984). One needs (1) the photon conversion mean free path as a function of its energy, (2) the particle energy loss rate for various emission mechanisms including the inverse Compton scattering of secondaries, and (3) the single particle photon emission spectrum. All of these are readily calculable given the "low" energy photon distribution $n(\omega)$ in the secondary region. In our model calculation (see Fig. 6), all we need as input for the initially interacting crossed beam is part of the spectrum of equation (7.1) between about 20 eV and 1 MeV. A test of the model is

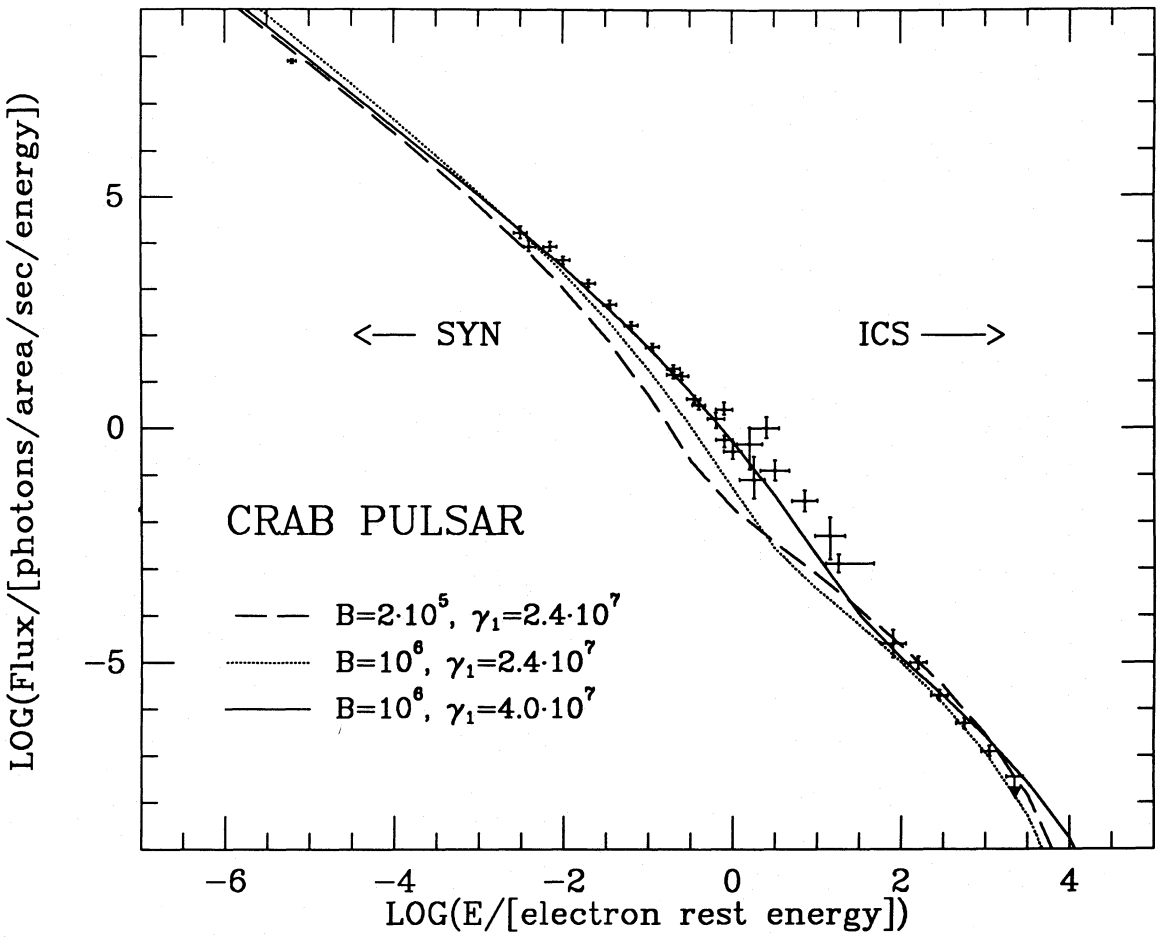

FIG. 6.—Calculated and observed spectra of the pulsed electromagnetic emission from the Crab pulsar. The theoretical spectra use the parameters discussed in § VII: $s = L = 10^8$ cm and $n(\hbar\omega \approx mc^2) = 10^{15}$ cm^{-3}. The dashed and dotted calculated spectra are those for $\gamma_1 = 2.4 \times 10^7$ with $B = 2 \times 10^5$ G and 10^6 G respectively; the solid curve is that for $B = 10^6$ G and $\gamma_1 = 4 \times 10^7$. All the spectra are normalized to fit the overall observed intensity. At X-ray frequencies, synchrotron radiation by the secondaries dominates the spectrum. At γ-ray frequencies, the photon spectrum is mainly from inverse Compton boosting of the lower energy synchrotron photons by the secondary pairs whose flow is opposite them. The dip in the theoretical spectrum at about a few MeV is where contributions from these two radiation mechanisms are comparable to each other. (Data taken from Oke 1969; Kestenbaum 1976; Bennet *et al.* 1977; Knight 1982; Mahoney, Ling, and Jacobson 1984).

whether what comes out is consistent with the input in this energy range and also reproduces the observed low-energy spectrum down 1 eV and the high-energy spectrum up to 1 GeV and above. Blumenthal and Gould (1970) have discussed the case of the inverse Compton spectrum and the energy loss rate of relativistic electrons in an isotropic background of photons. The extension of that discussion to the case of the mostly head-on collisions appropriate for the crossed beam geometry is straightforward.

As discussed in § VI, most of the Crab's gap power is likely to be carried out into the secondary region by curvature photons with energy ~3–30 GeV. Most of them will be converted into $e^{\pm}$ pairs which, because of their perpendicular motions as a result of finite intersecting angle at conversion between $\boldsymbol{B}$ and their ancestral photon, will synchrotron-radiate. Because of head-on collisions with the large flux of secondary photons, they will also inverse Compton scatter. In a magnetic field of about 10^6 G, the initial secondary GeV electrons ($\gamma \approx 10^3$–10^4) synchrotron-radiate into the frequency range of $\hbar\omega \lesssim \gamma^2\hbar\omega_B \approx 10^6$ eV. These synchrotron photons will be observed as the Crab's pulsed X-rays and optical photons. When the oppositely directed flow of secondary $e^{\pm}$'s encounters these synchrotron photons, a fraction will inverse Compton scatter into the energy range of $\hbar\omega \lesssim \gamma mc^2 \approx$ a few GeV.

In our model calculation for the Crab pulsar, the radius of curvature and the dimension of the outer magnetosphere are taken to be $\sim 10^8$ cm, and the secondary photon number density of equation (7.2) is $n(\hbar\omega \approx mc^2) = 10^{15}$ cm^{-3}. We assume that the primary gap e^+/e^-'s are monoenergetic, with $\gamma_1 = 2.4 \times 10^7$. Then the primary photon spectrum is that of curvature radiation whose characteristic energy is ~20 GeV. This is achieved for an outer gap with $\boldsymbol{E} \cdot \hat{\boldsymbol{B}} \approx 3 \times 10^6$ V cm^{-1} and $\Delta V \approx 3 \times 10^{14}$ V along a gap length of 10^8 cm. The results of the calculations for a magnetic field of 2×10^5 G (scaled as Ω^3 from that of Vela used in § IV) and 10^6 G (maximum light cylinder field for a pure dipole approximation) are shown in Figure 6. Also shown in Figure 6 is the spectrum in the case of $\gamma_1 = 4 \times 10^7$ (primary photon characteristic energy ~80 GeV, outer gap $\boldsymbol{E} \cdot \hat{\boldsymbol{B}} \approx 2 \times 10^7$ V cm^{-1}, and $\Delta V \approx 2 \times 10^{15}$ V) and $B \approx 10^6$ G. The total integrated power is normalized to fit observations. The calculated spectrum over nine orders of magnitude agrees very roughly with that measured but is off by a factor of several or more in some regions.

Because of our approximations to the geometry and the electrodynamics, it should be emphasized that a better spectral fit from fine tuning this calculation, though possible, does not necessarily provide more information about the gap or better support for the model.

VIII. OTHER KINDS OF RADIATION AND OTHER PULSARS

a) 10^{12}–10^{13} eV γ-*Rays*

The secondary e^+/e^- in Vela lose almost all their energy to synchrotron radiation. However, a small fraction is lost to inverse Compton scattering on the same soft photons which are Compton scattered by the primaries and which participate in the creation of secondaries by the pair coversion of primary γ-rays. The ration η of inverse Compton loss to synchrotron loss by secondaries is roughly $\eta \approx (\gamma^2 \sigma_T nc^2 \hbar\omega_{IR}) \times (\gamma_\perp^2 e^2 \omega_B^2)^{-1}$. This overestimates η at the largest γ where $\gamma^2 \omega_{IR} \sigma_T$ should be replaced by a smaller relativistic Compton form which effectively replaces σ_T by $\sim \sigma_P$. For Vela, with the parameters of §§ IV and V (observed emission region $\omega_B \approx 8 \times 10^{10}$ s^{-1}, $\hbar\omega_{IR} \approx 10^{-1}$ eV, $\gamma^2 n \sigma_T \approx 10^2 \gamma^2 L^{-1} \approx \gamma^2 10^{-8}$ cm^{-1}, $\gamma_\parallel^2 \approx 10$), $\eta \approx 10^{-2}$. Although this is a small fraction of the radiated γ-ray power, the inverse Compton boosted secondary photons can be in an energy range very much greater than the 3 GeV maximum for the secondary synchrotron radiation. The inverse Compton photons have energies up to the initial energy of secondary $e^\pm$, given in equation (5.3) as $E_1(\gamma)/2 \approx 5 \times 10^{12}$ eV. (It is characteristically $\sim[m^2c^4/\hbar\omega_{IR}]$.) Thus, for Vela (and for the Crab), about 10^{-2} of the gap-generated power should be radiated by secondaries in a spectrum which images that of the dominant synchrotron emission but is shifted up in energy by $\sim 10^3$, from a synchrotron cutoff ~ 3 GeV to an inverse Compton cutoff $\sim 6 \times 10^{12}$ eV. Absorption by further pair creation on the tertiary photons can reduce this upper cutoff, but Vela's outer magnetosphere magnetic field ($\sim 10^4$ G) is small enough to permit the escape of TeV γ-rays without pair conversion on $\boldsymbol{B}$ itself. Because these γ-rays come from the same secondaries as those that give the main synchrotron γ-ray and X-ray emission, they should be observed in pulses coincident in arrival time with the lower energy γ-ray ones. TeV pulses from Vela with the same pulse interpulse spacing as the γ-rays has been reported by Bhat *et al.* (1980).

The Crab-type mechanism of § VI does not give any e^-/e^+ with energies large enough to give 10^{12} eV γ-rays. These can only come from some admixture of Vela-type mechanisms in which the 10^{13} eV γ-rays will generally be absorbed by the IR-optical photons of the secondary radiation beams. The resulting $e^\pm$ pairs will give synchrotron radiation of characteristic energy $\hbar\omega_c \approx (\hbar\omega_1/mc^2)^2 \hbar\omega_B \approx 10^{12}$ eV. The main and great uncertainty in any quantitative estimate of the power in such photons is the unknown probability that such photons can escape without further absorption from $e^\pm$ production on the secondary optical photons through which they would normally pass to escape from the magnetosphere. This is expected to be possible only because of density fluctuations in the secondary flows. In addition. the Crab's outer magnetosphere B is expected to be almost 30 times larger than that of the Vela pulsar, so that inward-moving TeV γ-rays, which will have to pass through magnetic fields greater than 10^6 G as they traverse the magnetosphere, may be largely absorbed by pair creation in such B. Only the outward-directed TeV beams survive. Evidence for a least a single TeV γ-ray pulse coincident with the "main" pulse from the Crab has been given by Dowthwaite *et al.* (1984) and others.

b) *Radio Emission*

Vela's radio emission is presumed to originate in a part of the magnetosphere separated from, and uninfluenced by, the regions controlled by the outer gap. It was suggested elsewhere (Ruderman 1981) that the observed radio emission from Vela and the "precursor" beam from the Crab have a (not pair-related) similar origin near the stellar surface. The near surface magnetic field of a young neutron star may be quite irregular until the eddy current decay time in its crust ($\sim 10^6$ yr) permits simplification. Therefore, the open field lines of the stellar magnetic field, although reasonably dipolar in much of the outer magnetosphere, may have a complicated structure in several surface polar cap regions from which radio emission is beamed in several directions which bear no particular relation to the outer gap beams. Therefore we cannot deduce the timing interval between the high-energy γ-ray beams of Vela and its radio beam or between the pulse-interpulse beams of the Crab and its precursor radio beam. The pulse-interpulse radio beams from the Crab are coincident with the higher energy ones and thus would seem to come from the same secondary $e^\pm$ pairs. Density irregularities in the flow of secondaries can act like relativistically moving mirrors to scatter collectively a radio beam (generated much nearer the neutron star) which partly passes through the observed secondary emission region. The "mirror" would be moving in both directions along $\boldsymbol{B}$ with $v_\parallel/c = \pm(1 - \gamma_\parallel^{-2})^{1/2}$. The reflected beams would be approximately coincident with the secondary synchrotron emission from the plasma mirrors and have a frequency $\gamma_\parallel^2 \approx 10$ times that of the incident (precursor-like) radio frequency beams, a possibility not qualitatively in conflict with observation. This possibility for double-beamed frequency-boosted radio beam generation will be considered in a subsequent paper on Crab-like outer gaps.

We note finally that if an outer gap is present, an outward flow of ions would occur somewhere from any polar cap. If $\rho_0 = \boldsymbol{\Omega} \cdot \boldsymbol{B}/2\pi c > 0$, a net positive charge is expected to flow out from the polar cap along upward-bending field lines (and the outer gap generates e^+, in $e^\pm$ pairs, which flow back to the star on other open field lines). If $\rho_0 < 0$, electrons should flow out along the upward-curving field lines and be partly replenished by outer gap–created electrons flowing back to the polar cap on downward-curving open field lines. But, as discussed in CHR, the downward flow of electrons into the star will be approximately balanced by positive ions pulled from the star and accelerated by the column of negatively charged inflow. Therefore, models for near-surface radio frequency emission from young pulsars which are based on a presumed polar cap ion outflow (e.g., Ruderman 1981) may be applicable no matter what the sign of $\boldsymbol{\Omega} \cdot \boldsymbol{B}$ above the cap.

c) *Pair Flux Emission through the Light Cylinder*

Equation (5.16) can also be used to estimate the total number of tertiary $e^\pm$ created. Essentially all will flow out through the light cylinder, the outward-flowing ones directly, the inward-flowing ones after magnetic mirror reflection. With the same approximation as those which lead to equation (5.18),

$$F_3 \approx \frac{2\sigma_P}{Wc} \frac{4 \times 10^{34} \text{ ergs s}^{-1}}{m^2c^4} \int_{m^2c^4/3 \text{ GeV}}^{mc^2} d\omega' I(\omega') \,. \quad (8.1)$$

With an estimated integrated X-ray intensity for Vela below 500 keV of 10^{34} ergs s^{-1}, equation (8.1) gives $F_3 \approx 10^{36}$ s^{-1}. From observations of the synchrotron X-ray and radio nebula around Vela, the needed pulsar e^-/e^+ injection is estimated to be $\sim 10^{36}$ s^{-1} (Cheng 1984; Weiler and Panagia 1980; Helfand 1984).

For the Crab pulsar outergap, each of the $F_1 = 10^{33}$ s^{-1} e^+/e^- primaries radiates $\gamma_1 e^2/\hbar c \approx 10^5$ curvature γ-rays. Thus the flux of multi-GeV primary γ-rays $N_1 \approx 10^{38}$ s^{-1}. This gives a secondary $e^\pm$ flux $F_2 \approx 10^{38}$ s^{-1}. A calculation equivalent to that which gives equation (8.1) gives an additional factor of 10 for the $e^\pm$ flux of pair production from the crossed secondary beams. Thus $F_3 \approx 10^{39}$ s^{-1} for the total $e^\pm$ flux produced in the Crab's outer magnetosphere, somewhat larger than is needed to account for the nebular emission (see Kennel and Coroniti 1984).

d) Superenergetic Ion Beams: 10^{15} eV γ-Rays?

If $\rho_0 < 0$ above the polar cap, electrons are sent down onto the cap by the outer gap. Oppositely charged positive ions (or protons) which largely cancel the incoming negatively charged column are then expected to be sucked up from the cap (cf. CHR I, Arons 1983). These will reach the null surface end of the outer gap and be accelerated without significant loss along the entire gap length. They will, therefore, acquire the full gap potential drop before being ejected at the light cylinder gap end. Therefore if Vela has a polar cap with $\rho_0 < 0$, it should also be the source of two 10^{15} eV (per nucleon) ion beams with a power of 10^{35} ergs s^{-1} (and smaller latitudinal spread than the fan-beamed electromagnetic radiation). A similar particle beam from the Crab pulsar, if its $\rho_0 < 0$, would carry even more power ($\sim 10^{36}$ ergs s^{-1}) and particle energy. Effects of these superenergetic particle beams could be detected if there were sufficient matter near the pulsar to intercept the beams by proton or nucleon collisions. The prompt two γ-ray decay of π^0 mesons from such collisions (or neutrinos from charged meson decays) would be of uniquely high energy (up to or exceeding 10^{15} eV), since radiation reaction would keep any e^+/e^- from acquiring enough energy to be a possible source. A thin intercepting target would convert the nucleon energy into γ-rays and neutrinos from a single collision but not degrade the γ-ray energies by subsequent interactions. The additional latitude spread of the γ-rays would then be only of order $\gamma_{CM}^{-1} \approx \gamma_p^{-1/2} \approx 10^{-3}$, where γ_p is the Lorentz factor of the gap-accelerated nucleons. Since the nucleons, emitted only from the outer end of the accelerating gap, have a small initial spread in polar angles (which may be even more diminished by aberration effects at $r = c\Omega^{-1}$), the beam decay products will usually not be observed. When they are, the beam power inferred will, therefore, generally be exaggerated. A suitable target for the detection of such superenergetic particle beams does not seem to exist near Vela. For the Crab pulsar, such an energetic proton beam can give photoproduced π^0 mesons when passing through the pulsar's very strong soft X-ray beam. A 0.3 keV X-ray will be seen as a 300 MeV γ-ray by a 10^{15} eV proton, an energy where the π^0 photoproduction cross section peaks near 3×10^{-28} cm^2. In the magnetosphere, the very soft X-ray flux is sufficient to give $\sim 10^{33}$ s^{-1} 10^{15} eV γ-rays if such a proton beam passes through the Crab's outer gap. However, if such γ-rays cross a local magnetic field at an angle $\hat{\theta}$ such that $\hat{\theta}B \lesssim 10^3$, they will create Sturrock pairs. Therefore such π^0 production within the Crab light cylinder is probably unimportant.

e) Polar Cap Heating

Particle flow directed along open field lines down onto the surface of the star can heat the polar cap. For Vela there is no detected modulated X-ray signal (Harnden *et al.* 1985) from such heating which limits heated polar cap luminosity to $L_x(\text{polar cap}) < 10^{32}$ ergs s^{-1}.

Although most of the Vela gap power ($\sim 10^{35}$ ergs s^{-1}) is initially transferred to secondaries, essentially all the secondary energy would be synchrotron-radiated away before the surface (with $B \approx 3 \times 10^{12}$G) is approached. Primary $e^+(e^-)$ flowing through the null surface end of the outer gap toward the star will already have an energy greatly reduced from the mean $e^\pm$ energy deep within the gap, since $\boldsymbol{E} \cdot \hat{\boldsymbol{B}}$ falls off to zero at that gap end on a length scale of the gap width (cf. Fig. 6 of CHR I) which is much larger than the $e^\pm$ mean free path ($\lambda \approx 10^{-2}L$) for inverse Compton scattering. Even more important, there is no reason for that scattering to cease abruptly at the gap inner end. Thus, for stellar inflow of primaries from the gap,

$$\left|\frac{d\gamma_1}{ds}\right| = -\frac{\gamma_1^2}{\lambda}\frac{\hbar\omega_{IR}}{mc^2}. \tag{8.2}$$

After moving an additional length $\hat{L} = \kappa L$, their γ_1 will drop to $(mc^2/\hbar\omega_{IR})(\lambda/\kappa L) \approx 10^5$ for $\kappa = \frac{1}{2}$. For a primary flux $F_1 \approx 3 \times 10^{32}$ s^{-1} (cf. § IV), the total power from primary $e^+(e^-)$ impacting on the polar cap would then be $\sim 3 \times 10^{31}$ ergs s^{-1}.

We note, however, that any significant flow of protons (or positive ions other than e^+) pulled into the gap from the light cylinder end and accelerated through the gap would result in unacceptable polar cap heating, since the heavy primaries would then acquire (and not subsequently lose) the full gap potential drop $e\Delta V \approx 10^3$ ergs. Ions flowing out from the polar cap of a young warm Vela pulsar would not be largely stripped of their electrons. Thermal X-ray photoelectric dissociation can then create a stripped ion-electron plasma which limits subsequent potential drops to less than 10^{10} V. The accelerated electron backflow onto the polar cap could then deposit a maximum power there of $\sim F_1(\text{max})eV \approx 10^{31}$ ergs s^{-1}, comfortably less than the present upper bound for polar cap thermal emission. However, radio emission models for young Vela-type pulsars in which a near-surface $e^\pm$ plasma must be generated generally need potential drops $V \approx 10^{12}$ V there, so that the power deposited from $e^+(e^-)$ backflow onto surface [$eVF_1(\text{max}) \approx 10^{33}$ ergs s^{-1}] could be embarrassingly large.

f) Other Rapidly Spinning Pulsars

Key pulsar parameters for outer gap formation involve the potential drop that can be mobilized in such a gap and the created particle flow through it. Both are roughly proportional to $\Omega^2 B_s$, where B_s is the surface dipole magnetic field. Pulsars with $\Omega^2 B_s$ similar to that of Vela and the Crab include the young pulsars PSR 1509−58 (Seward and Harnden 1982; Manchester, Tuohy, and D'Amico 1982), PSR 0540−693 (Seward, Harnden, and Helfand 1984) and the, probably, very old pulsar (with much weaker B_s but much larger Ω) PSR 1937+214 (the "millisecond pulsar," Backer *et al.* 1982). Spinning magnetic white dwarfs may also generate an outer magnetosphere $\boldsymbol{E} \cdot \hat{\boldsymbol{B}}$ and particle flow similar to those of Vela if $(\sim B_s R_{WD}^3)\Omega_{WD}^2$ is comparable to Vela's. This would be achieved for a magnetized white dwarf with $B_s = 10^8$ G, $R_{WD} = 10^9$ cm, and a 16 s period.

Even Vela might give significantly different observed radi-

ation if our angle of viewing were to be so different that the observable emission region lay very much closer to (further from) the star. Pulse interpulse separation would be smaller (larger). A stronger observed local B could be greatly lower than ω_c of equation (5.9), the frequency for the spectral break. Vela might, therefore, have a detectable optical beam from the synchrotron radiation of its secondaries if more favorably viewed. The approximate symmetry between the two beams seen in each stellar rotation would be expected to disappear if the observed region were to be close to a gap and only a very small current of primary e^+ or e^- flowing away from the gap end has space to build up. Finally, there is the possibility that Vela's beamed γ-ray luminosity might be even stronger if its γ-ray emission from another part of its gap-controlled region were to be observed. Equations (4.10) and (4.13a) suggest that gap power unit length might possibly increase with increasing B, but this ignores necessary connections between the current flow and boundary field line of different gap stretches. If Vela-type pulsars are indeed much brighter γ-ray sources when observed from cetain directions, then a subset of such pulsars may be candidates for some of the 21 unidentified *COS B* γ-ray sources (Bignami and Hermsen 1983) in our galaxy.

Most of the research summarized in this paper was carried out at Columbia University with the support from the National Science Foundation under grant PHY 80-23721. We are happy to thank Jonathan Arons for criticism and stimulation, M. R. is grateful to Sidney Drell and the theoretical group at SLAC for their very kind hospitality. Part of C. H.'s work at the University of California was also supported by the NSF under grant AST 83-17462.

APPENDIX

SECONDARY e^+/e^- AND PHOTON SPECTRA

In this Appendix, we set up the basic equations for the distribution functions of the electrons in the secondary region which we use to calculate the secondary emission spectrum in § VII. The primary electron distribution is given by an F_1:

$$F_1(\boldsymbol{x}_1, \boldsymbol{p}_1) = \frac{\text{number of electron}}{d^3\boldsymbol{x}_1\, d^3\boldsymbol{p}_1} . \tag{A1}$$

Each of these electrons will emit photons with a spectrum $dN(\boldsymbol{k}_1, \boldsymbol{p}_1)/dtd^3\boldsymbol{k}_1$. These photons will propagate out of the primary region (of course, some of them convert within the primary region to close the gap), and the primary photon number distribution function is given by

$$\begin{aligned} N_1(\boldsymbol{x}_2, \boldsymbol{k}_1) &= \frac{\text{number of photons}}{d^3\boldsymbol{x}_2/d^3\boldsymbol{k}_1} \\ &= \int d^3\boldsymbol{x}_1\, d^3\boldsymbol{p}_1\, F_1(\boldsymbol{x}_1, \boldsymbol{p}_1)\, \frac{dN(\boldsymbol{k}_1, \boldsymbol{p}_1)}{dtd^3\boldsymbol{k}_1}\, \frac{\delta^2[\hat{n}(\boldsymbol{x}_1 - \boldsymbol{x}_2) - \hat{n}(\boldsymbol{k}_1)]}{c\,|\boldsymbol{x}_1 - \boldsymbol{x}_2|^2} . \end{aligned} \tag{A2}$$

These emitted photons will have a mean free path λ for converting into $e^{\pm}$ pairs. The rate of conversion at $\boldsymbol{x}_2$ per unit volume per unit time ($\mathscr{P}_c$) for a photon emitted at $\boldsymbol{x}_1$ is given by

$$\begin{aligned} \mathscr{P}_c(\boldsymbol{x}_1, \boldsymbol{x}_2, \boldsymbol{k}_1, \boldsymbol{p}_2) &= \frac{\text{Probability of conversion at } \boldsymbol{x}_2 \text{ into } \boldsymbol{p}_2}{dtd^3\boldsymbol{p}_2} \\ &= \left(\frac{c}{\lambda}\right) \exp\left(-\int \frac{dl}{\lambda}\right) \frac{d\mathscr{P}}{d^3\boldsymbol{p}_2} , \end{aligned} \tag{A3}$$

where $d\mathscr{P}/d^3\boldsymbol{p}_2$ is the probability of photon $\boldsymbol{k}_1$ converting into electron $\boldsymbol{p}_2$ and the integration is from $\boldsymbol{x}_1$ to $\boldsymbol{x}_2$. The secondary electron generation rate $G_2(\boldsymbol{x}_2, \boldsymbol{p}_2)$ is given by

$$\begin{aligned} G_2(\boldsymbol{x}_2, \boldsymbol{p}_2) &= \frac{\text{number of created electrons with } \boldsymbol{p}_2}{d^3\boldsymbol{x}_2\, d^3\boldsymbol{p}_2\, dt} \\ &= \int d^3\boldsymbol{k}_1\, N_1(\boldsymbol{x}_2, \boldsymbol{k}_1)\mathscr{P}_c(\boldsymbol{k}_1, \mathbf{p}_2) . \end{aligned} \tag{A4}$$

The secondary electron density distribution, defined as

$$F_2(\boldsymbol{x}_2, \boldsymbol{p}_2) = \text{number of electrons}/d^3\boldsymbol{x}_2\, d^3\boldsymbol{p}_2 , \tag{A5}$$

is related to the electron generation function through the continuity equation

$$\frac{d}{dx}\left[\dot{x}F_2(\boldsymbol{x}_2, \boldsymbol{p}_2)\right] + \frac{d}{dp}\left(\dot{p}F_2[\boldsymbol{x}_2, \boldsymbol{p}_2]\right) = G_2(\boldsymbol{x}_2, \boldsymbol{p}_2) . \tag{A6}$$

Finally, the secondary radiation spectrum is given by

$$P_{\text{total}}(\boldsymbol{k}_2) = \int d^3\boldsymbol{x}_2\, d^3\boldsymbol{p}_2\, F_2(\boldsymbol{x}_2, \boldsymbol{p}_2)[dP(\boldsymbol{p}_2, \boldsymbol{k}_2)/d^3\boldsymbol{k}_2] , \tag{A7}$$

where $dP(\boldsymbol{p}, \boldsymbol{k})/d^3\boldsymbol{k}$ is the single particle radiation spectrum of the specific radiation mechanism.

Those photons with conversion optical depth less than unity will reach an observer and contribute to the observed spectrum. The primary photons generally have higher energy and shorter conversion mean free path. The secondary region is optically thick for typical primary photons from both the Crab and Vela gaps. We model the Crab secondary emission spectrum from the observed one. We use the following simplification to obtain an integrable secondary distribution, based on which the secondary emission spectra is calculated.

First, assume that the primary e^+/e^- are distributed in a spatially small region compared to both the gap and the secondary region. Thus we first approximate the spatial dependence of F_1 by a δ-function: $\delta[w(x, y, z)]$, where $w = 0$, represents the surface on which this maximum power region lies. In the geometry used in the electrostatic analysis, w corresponds to the coordinate z.

Second, the radiation reaction limit regulates the primary particle distribution, so that it is almost monoenergetic. Thus we approximate the primary electrons' energy distribution as a δ-function, i.e., $\delta(\gamma_1 - \gamma_0)$.

Third, the strong magnetic field collimates the electron motion almost perfectly. Thus the directional dependence on momentum is again δ-function–like. As a result, the primary electrons' distribution $F_1(\boldsymbol{x}_1, \boldsymbol{p}_1)$ can be written as

$$F_1(\boldsymbol{x}_1, \boldsymbol{p}_1) \approx Q\delta[w(\boldsymbol{x}_1)]\delta^2[\hat{n}(\boldsymbol{p}_1) - \hat{B}]\delta(\gamma_1 - \gamma_0)/\gamma_1 p_1 , \tag{A8}$$

where $\hat{n}(\boldsymbol{p}_1)$ and $\hat{B}$ are the direction of the primary electron momentum and local magnetic field. Q has the dimension of number of particles per area and corresponds to the total number of primary particles passing through the total primary area. The normalization factor Q is given by $Q \approx F_1/Wc$, where W is the beadth of the gap.

Fourth, the primary electrons' high-energy emission spectrum is simplified by using the (good) approximation that a relativistic charge emits photons almost completely in the forward direction. Thus the single particle spectrum can be rewritten as

$$\begin{aligned} dN/dt/d^3\boldsymbol{k}_1 &= [dN(\gamma, \omega_1)/dt d\omega_1\, \omega_1^2]\{\delta^2[\hat{n}(\boldsymbol{k}_1) - \hat{n}(\boldsymbol{p}_1)]\} \\ &= [dP_1(\gamma_1, \omega_1)/d\omega_1 \omega_1^3]\{\delta^2[\hat{n}(\boldsymbol{k}_1) - \hat{n}(\boldsymbol{p}_1)]\} , \end{aligned} \tag{A9}$$

where $dP_1(\omega_1, \gamma)/d\omega_1$ is the single particle emission power spectrum of the primary machine. After substituting equations (A8) and (A9) into equation (2) and carrying out the integration over the δ-functions, one gets

$$N_1(\boldsymbol{x}_2, \boldsymbol{k}_1) = Q\left[\frac{dP_1(\gamma_0, \omega_1)}{d\omega_1}\right]\left\{\frac{\delta^2[\hat{n}(\boldsymbol{k}_1) - \hat{n}(\boldsymbol{x}_2)]}{c\omega_1 \sin\theta}\right\} , \tag{A10}$$

where the unit vector $\hat{n}(\boldsymbol{x}_2)$ is the direction along the propagation path which passes through $\boldsymbol{x}_2$ and is tangentially extended from a field line on the primary surface $w = 0$; θ is the angle between $\hat{n}(\boldsymbol{x}_2)$ and the local field line at $\boldsymbol{x}_2$. The $1/\sin\theta$ factor comes from the integration Jacobian $|d(\boldsymbol{x}_2 - \boldsymbol{x}_1)/dw|$.

Fifth, $e^\pm$ pairs created by γ-γ collisions generally share the energy and momentum of the dominant photon, which usually has an energy very much in excess of mc^2. For simplicity, we assume that the production spectrum has a δ-function distribution:

$$d\mathscr{P}/d^3\boldsymbol{p}_2 \approx 2\delta^3(\boldsymbol{p}_2 - \boldsymbol{k}_1/2) . \tag{A11}$$

Using the variables $(\gamma_\parallel, \gamma_\perp)$, equation (A11) can be rewritten as

$$d\mathscr{P}/d\gamma_\parallel\, d\gamma_\perp \approx 2\gamma_\parallel\, \delta(\gamma - \omega_1/2)\delta[\gamma_\parallel - \gamma_{\parallel,0}(\boldsymbol{x}_2)] , \tag{A12}$$

where $1/\gamma_{\parallel,0}(\boldsymbol{x}_2)$ corresponds to the locally defined angle θ used in equation (A10).

After incorporating equations (A3), (A10), and (A12) into equation (A4) and carrying out the integration over the δ-functions, one gets

$$G_2(\boldsymbol{x}_2, \gamma_\parallel, \gamma_\perp) = Q2\gamma_\parallel^2\, \frac{\exp(-\int dl/\lambda)}{\lambda\gamma}\left[\frac{dP_1(\gamma_0, 2\gamma)}{d(2\gamma)}\right]\delta\left(\frac{\gamma_\parallel - s}{l}\right) , \tag{A13}$$

where s is the radius of curvature, l the propagation path, and the relation $\sin\theta \approx \gamma_\parallel^{-1}$ has been used.

Sixth, the strong magnetic field confines the relativistic particles to move along the magnetic field, with $\dot{\boldsymbol{x}} \approx c\hat{B}$. Also, assuming almost constant creation of $e^\pm$ along the field line results in similar spatial dependence for F_2 and G_2. After integrating over the secondary region, one arrives at

$$d/d\gamma_\perp[\dot{\gamma}_\perp F_2(\gamma_\parallel, \gamma_\perp)] = G_2(\gamma_\parallel, \gamma_\perp) . \tag{A14}$$

$G_2(\gamma_\parallel, \gamma_\perp)$ is obtained by the integration over $\boldsymbol{x}_2$ in equation (A13):

$$G_2(\gamma_\parallel, \gamma_\perp) \approx 2QA_2\, s\left[\frac{\exp(-s/\lambda\gamma_\parallel)}{\lambda\gamma\gamma_\parallel}\right]\left[\frac{dP_1(\gamma_0, 2\gamma)}{d(2\gamma)}\right] , \tag{A15}$$

where A_2 is approximately the emission area of the plane whose normal is in the direction of the radius of curvature. The quantity λ

is generally a function of γ. The particle distribution F_2 comes from the integration

$$F_2(\gamma_\parallel, \gamma_\perp) = \left[\int_{\gamma_\perp}^{\infty} d\gamma_\perp G_2(\gamma_\parallel, \gamma_\perp) \right] \Big/ |\dot{\gamma}_\perp| . \tag{A16}$$

Finally, one has to take into account the effect of the finite size of the magnetosphere. Secondary particles with relativistic energy stay in the Crab magnetosphere for $\sim r_{LC}/c \approx 10^{-2}$ s. During this time, they may not have lost all their energy. The pulsed radiation comes from a region rigidly corotating with the star within the light cylinder. We assume that electrons that flow outside the corotating magnetosphere no longer contribute to the pulsed emission. The time scale for a particle to reach energy $(\gamma_\parallel, \gamma_\perp)$ while losing energy at a rate $\dot{\gamma}$ is

$$\tau_{life} \approx \gamma/\dot{\gamma} = \gamma_\perp/\dot{\gamma}_\perp . \tag{A17}$$

Here $\dot{\gamma}$ is the sum of all the energy loss rates from all possible secondary radiation mechanisms. For the secondary particles to contribute to the pulsed emission, they must have a radiation lifetime shorter than the time for them to traverse the magnetosphere τ_{tr}, with

$$\tau_{tr} \approx \frac{L_{tr}}{c} = 0.003 \left(\frac{L_{tr}}{10^8 \text{ cm}} \right) \text{ s} , \tag{A18}$$

where L_{tr}, approximately equal to the light cylinder radius, is the size of the magnetosphere. This leads to a cutoff of the secondary particle distribution which can affect the pulsed emission. We include a step function cutoff independent of the particle generation spectrum. This gives (cf. eq. [A16]):

$$F_2(\gamma_\parallel, \gamma_\perp) = \left[\int_{\gamma_\perp}^{\infty} d\gamma_\perp G_2(\gamma_\parallel, \gamma_\perp) \right] \Theta[\tau_{tr} - \tau_{life}(\gamma_\parallel, \gamma_\perp)] \Big/ |\dot{\gamma}_\perp| . \tag{A19}$$

After these simplifications, including the consideration of the finite magnetosphere, the problem of the secondary radiation becomes the following: given an assumed primary mechanism, one gets a primary e^+/e^- energy (γ_0) and a primary radiation (curvature radiation or inverse Compton scattering) spectrum $dP_1/d\omega$. From a $\gamma + \gamma$ conversion mechanism, the secondary particle generation spectrum G_2 is obtained from equation (A15). Taking into account all possible energy loss mechanisms (synchrotron radiation and inverse Compton scattering) and their contribution to $\dot{\gamma}_\perp$ and τ_{life}, F_2 is given by equation (A19). The observed secondary spectrum (cf. eq. [A7]) can now be found from

$$P_{total}(\omega) = \int d\gamma_\parallel \, d\gamma_\perp F_2(\gamma_\parallel, \gamma_\perp)[dP_2(\gamma_\parallel, \gamma_\perp, \omega)/d\omega] , \tag{A20}$$

with $dP_2(\gamma_\parallel, \gamma_\perp, \omega)/d\omega$ the total single particle emission spectrum of the various emission mechanisms.

REFERENCES

Albats, P. Frye, G. M., Jr., and Thomson, G. B. 1974, *Nature*, **251**, 400.
Arons, J., 1983, in *Proc. Workshop on Electron-Positron Pairs in Astrophysics*, ed. M. L. Burns, A. K. Harding, and R. Ramaty (New York: AIP), p. 163.
Backer, D., Kulkarni, S., Heiles, C., Davis, M., and Goss, W. 1982, *Nature*, **300**, 615.
Bennet, K., *et al.* 1977, *Astr. Ap.*, **61**, 279.
Bhat, P. N. Gupta, S. K., Ramana Murthy, P. V., Sreekantan, B. V., Tonwar, S. C., and Viswanath, P. R. 1980, *Astr. Ap.*, **81**, L3.
Bignami, G. F., and Hermsen, W. 1983, *Ann. Rev. Astr. Ap.*, **21**, 67.
Blumenthal, G. R., and Gould, R. J. 1970, *Rev. Mod. Phys.*, **42**, 237.
Cheng, A., Ruderman, M. A., and Sutherland, P. G. 1976, *Ap. J.*, **203**, 209.
Cheng, K. S. 1984, Ph.D. thesis, Columbia University.
Cheng, K. S., Ho, C., and Ruderman, M. A. 1985, *Ap. J.*, **300**, 500 (CHR I).
Dowthwaite, J. C., Harrison, A. B., Kirkman, I. W., Macrae, H. J., McComb, T. J. L., Orford, K. J., Turver, K. E., and Walmsley, M. 1984, *Ap. J. (Letters)*, **286**, L35.
Harnden, F. R. Jr., Grant, P. D., Seward, F. D., and Kahn, S. M. 1985, *Ap. J.*, **299**, 828.
Heitler, W. 1960, *The Quantum Theory of Radiation* (London: Oxford).
Helfand, D. 1984, *Adv. Space Res.*, Vol. **3**, No. 10–12, p. 29.
Ho. C. 1984, Ph.D. thesis, Columbia University.
Kanbach, G. *et al.* 1980, *Astr. Ap.*, **90**, 163.
Kennel, C. F., and Coroniti, F. V. 1984, *Ap. J.*, **283**, 710.
Kestenbaum, H. L., Ku, W., Novick, R., and Wolff, R. S. 1976, *Ap. J. (Letters)*, **203**, L57.
Knight, F. K. 1982, *Ap. J.*, **260**, 538.
Knight, F. K., Matteson, J. L., Peterson, L. E., and Rothschild, R. E. 1982, *Ap. J.*, **260**, 553.
Mahoney, W. A., Ling, J. C., and Jacobson, A. S. 1984, *Ap. J.*, **278**, 784.
Manchester, R. N., Tuohy, I. R., and D'Amico, N. 1982, *Ap. J. (Letters)*, **256**, L45.
Oke, J. B. 1969, *Ap. J. (Letters)*, **156**, L49.
Ruderman, M. A. 1981, in *IAU Symposium 95, Pulsars*, ed. W. Sieber and R. Wielebinski (Dordrecht: Reidel), p. 87.
Seward, F. D., and Harnden, F. R., Jr. 1982 *Ap. J. (Letters)*, **262**, L31.
Seward, F. D., Harnden, F. R., Jr., and Helfand, D. J. 1984, *Ap. J. (Letters)*, **287**, L19.
Sturrock, P. 1971, *Ap. J.*, **164**, 529.
Tümer, O. T., Dayton, B., Long, J., O'Neill, T., Zych, A., and White, R. S. 1984, *Nature*, **310**, 214
Weiler, K. W., and Panagia, N. 1980, *Astr. Ap.* **90**, 269.

K. S. CHENG: Department of Physics, University of Illinois, Urbana, IL 61801

C. HO: Astronomy Department, University of California, Berkeley, CA 94720

M. RUDERMAN: Department of Physics, Columbia University, New York, N.Y. 10027